Reviews in Mineralogy & Geochemistry
Vol. 61, pp. 231-264, 2006

Chemical Bonding in Sulfide Minerals

David J. Vaughan

School of Earth Atmospheric and Environmental Sciences
and Williamson Research Centre for Molecular Environmental Science
University of Manchester
Manchester, United Kingdom
e-mail: david.vaughan@manchester.ac.uk

Kevin M. Rosso

Chemical Sciences Division
and W. R. Wiley Environmental Molecular Sciences Laboratory
Pacific Northwest National Laboratory, P. O. Box 999, MSIN K8-96
Richland, Washington, 99352, U.S.A.
e-mail: kevin.rosso@pnl.gov

INTRODUCTION

An understanding of chemical bonding and electronic structure in sulfide minerals is central to any attempt at understanding their crystal structures, stabilities and physical properties. It is also an essential precursor to understanding reactivity through modeling surface structure at the molecular scale. In recent decades, there have been remarkable advances in first principles (*ab initio*) methods for the quantitative calculation of electronic structure. These advances have been made possible by the very rapid development of high performance computers. Several review volumes that chart the applications of these developments in mineralogy and geochemistry are available (Tossell and Vaughan 1992; Cygan and Kubicki 2001).

An important feature of the sulfide minerals is the diversity of their electronic structures, as evidenced by their electrical and magnetic properties (see Pearce et al. 2006, this volume). Thus, sulfide minerals range from insulators through semiconductors to metals, and exhibit every type of magnetic behavior. This has presented problems for those attempting to develop bonding models for sulfides, and also led to certain misconceptions regarding the kinds of models that may be appropriate.

In this chapter, chemical bonding and electronic structure models for sulfides are reviewed with emphasis on more recent developments. Although the fully *ab initio* quantitative methods are now capable of a remarkable degree of sophistication in terms of agreement with experiment and potential to interpret and predict behavior with varying conditions, both qualitative and more simplistic quantitative approaches will also be briefly discussed. This is because we believe that the insights which they provide are still helpful to those studying sulfide minerals. In addition to the application of electronic structure models and calculations to solid sulfides, work on sulfide mineral surfaces (Rosso and Vaughan 2006a,b) and solution complexes and clusters (Rickard and Luther 2006) are discussed in detail later in this volume.

IONIC AND COVALENT BONDS

As with all crystalline solids, representation using a simple ionic model in which the ions are considered to be charged spheres of a particular radius has proved useful in gaining a

1529-6466/06/0061-0005$05.00 DOI: 10.2138/rmg.2006.61.5

qualitative understanding of sulfide crystal structures. As discussed in more detail elsewhere in this volume (Makovicky 2006), the Shannon crystal radius of the S^{2-} ion (1.70 Å; Shannon 1981) which dominates in sulfide minerals is significantly greater than that of the O^{2-} ion of oxides and silicates, and the sulfide ion is more polarizable. Nevertheless, concepts such as the (cubic or hexagonal) close packing of anion spheres are also useful in understanding sulfide crystal structures. However, such approaches do not yield information on electronic structure or the subtleties of chemical bonding and will not be discussed in detail in this chapter. For further discussion, readers are referred to Vaughan and Craig (1978) and the very detailed analysis of sulfide structures and crystal chemistry provided by Makovicky (2006; this volume).

The qualitative theories of covalent bonding such as the hybridization of atomic orbitals have also been applied to sulfides, emphasizing the directionality of metal-sulfur bonds and significant delocalization of the electrons involved in bonding. As with the purely ionic approach, the usefulness of concepts derived from valence bond theory has largely been in gaining an understanding of crystal structures. Again, in the detailed discussion of crystal structures elsewhere in this volume (Makovicky 2006) use is made of these concepts in understanding structural principles. Also, fuller accounts of such approaches are provided by Vaughan and Craig (1978).

As discussed in detail below, both qualitative and quantitative modeling of bonding and electronic structure now center on molecular orbital and band theories, although for transition metal sulfides, the ligand (or crystal) field theories have also provided useful insights. Atomistic modeling, a quantitative approach developed from the ionic view has also, perhaps surprisingly, proved useful for certain applications, as described below.

LIGAND FIELD THEORY

The ligand field and crystal field theories have played an important role in the development of geochemistry (see Burns 1993 for a full account). In crystal field theory, the effects of the anions surrounding a transition metal cation on the energies of its *d*-electrons are modeled. Whereas in crystal field theory, these anions (S^{2-} ions in most sulfides) are treated as point charges, in ligand field theory, account is taken of the covalent contribution to metal-anion bonding through overlap between metal and anion orbitals. These theories therefore provide descriptions of only the *d*-electrons in the system being considered. As the transition metal sulfides are amongst the most important of this mineral group, the ligand field approach has yielded some useful insights, although a further limitation is that the *d*-electrons are treated as *localized* on the cations, whereas some sulfides exhibit considerable *d*-electron *delocalization*.

Hulliger (1968) and Nickel (1968, 1970) applied a ligand field model to explain the structural stabilities of certain disulfide and diarsenide minerals (see also Vaughan and Craig 1978; Burns 1993 for review). The transition metal disulfides containing S-S (and S-As or As-As) dimers exist in four principal structure-types characterized by pyrite, marcasite, arsenopyrite and loellingite (see Makovicky 2006). In each of these structures the metals are octahedrally coordinated to six anions which are, in turn, linked to other anions. However, in pyrite the octahedra only share corners, whereas in arsenopyrite, loellingite and marcasite, they share edges lying in the (001) plane. Relative to marcasite, loellingite has a compressed *c*-axis whereas arsenopyrite has alternate short and longer metal-metal distances along *c* (Fig. 1). The outer electron distribution in iron ($3d^6\ 4s^2$) indicates that in FeS_2, the *d*-electrons are not involved in metal-sulfur bonding (in terms of a simple ionic or covalent model). However, replacement of a sulfur by arsenic as in FeAsS results in a deficit of one electron per formula unit. If cation-anion electron pair bonds are to be maintained, a *d*-electron must be used in bonding. In $FeAs_2$, two such *d*-electrons will be required to maintain the electron pair bonds.

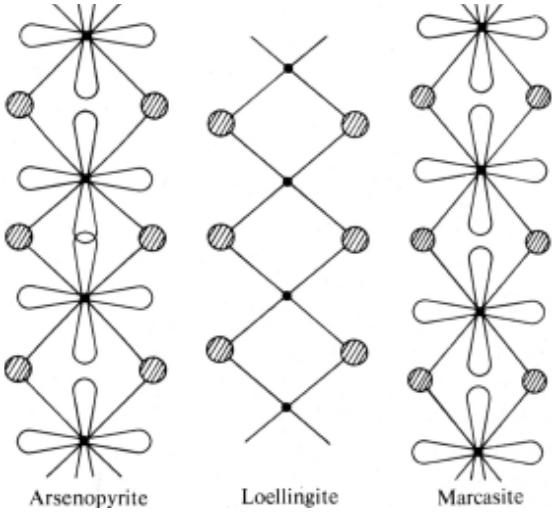

Figure 1. Proposed interactions of the t_{2g} orbitals (Fe 3*d*) along the direction parallel to the *c*-axis in arsenopyrite (FeAsS) and in marcasite (FeS_2); in loellingite ($FeAs_2$) this orbital would be empty. (Redrawn after Nickel 1970).

Magnetic and Mössbauer data indicate that pyrite and marcasite contain low-spin Fe^{2+} (t_{2g}^6) (see Pearce et al. 2006, this volume). However, in marcasite the octahedral edges are shared, making interaction between adjacent iron atoms along the *c*-axis possible, particularly as this is the direction of one of the t_{2g} orbital sets (Fig. 1). In fact, the angle subtending the shared octahedral edge (82°) indicates mutual repulsion of the filled *d*-electron clouds. In $FeAs_2$, there are four *d*-electrons not involved in bonding and they cannot achieve spin pairing if placed into the three t_{2g} orbitals. If the four electrons are paired into two of these orbitals (Pearson 1965), complete spin pairing will be achieved. The orbital parallel to the *c*-axis is the obvious choice for the empty orbital. This could explain the contraction along the *c*-axis (Fe-Fe distance 2.85 Å in loellingite, 3.38 Å in marcasite) and the low magnetic moment reported for iron in loellingite (Wintenberger 1962). In FeAsS, the iron atom has five *d*-electrons not involved in metal-anion bonding and spin-pairing can only be achieved if an unpaired electron in a t_{2g} orbital on one atom is paired with an equivalent electron on the adjacent metal atom across the shared octahedral edge. The alternate short (2.89 Å) and long (3.53 Å) metal-metal distances along the *c*-axis in arsenopyrite result. Again magnetic evidence supports this model (Wintenberger 1962). These structural relationships are all illustrated in Figure 1.

Various iron, cobalt and nickel chalcogenides having the same or very similar structures can be considered using the same models (see Table 1). For example, CoAsS and $NiAs_2$ (cobalt having a $3d^7\,4s^2$ configuration, nickel $3d^8\,4s^2$) are isoelectronic with FeS_2 and have a modified pyrite and a marcasite structure, as the minerals cobaltite (CoAsS) and rammelsbergite ($NiAs_2$) respectively. $CoAs_2$ is isoelectronic with FeAsS and does, indeed, crystallize with the arsenopyrite structure. Compounds with seven (CoS_2, NiAsS) and eight (NiS_2) nonbonding *d*-electrons crystallize with a pyrite or closely related structure as the model would predict. The additional electrons go into the two e_g orbitals which are proximal to the ligands and tend to have a repulsive effect, increasing metal-sulfur distances and the overall unit cell dimensions.

The stability of the marcasite structure, despite the repulsion of metal atoms across the shared edge, has been suggested as being due to a complex bonding scheme involving second-nearest-neighbor sulfur atoms (Pearson 1965). The anion pairs in this structure tend to form

Table 1. The crystal structures of the dichalcogenides in relation to *d*-electron configuration (modified from Nickel 1970).

Composition	Mineral name	# of *d*-electrons	Structure-type[a]
$FeAs_2$	Loellingite	4	Loellingite
$FeSb_2$	—	4	Loellingite
FeAsS	Arsenopyrite	5	Arsenopyrite
FeSbS	Gudmundite	5	Arsenopyrite
$CoAs_2$	Safflorite	5	Arsenopyrite
FeS_2	Pyrite	6	Pyrite
CoAsS	Cobaltite	6	Pyrite
CoSbS	—	6	Pyrite
FeS_2	Marcasite	6	Marcasite
FeS_2	Ferroselite	6	Marcasite
$FeTe_2$	Frohbergite	6	Marcasite
$NiAs_2$	Rammelsbergite	6	Marcasite
CoS_2	Cattierite	7	Pyrite
$CoSe_2$	Trogtalite	7	Pyrite
NiAsS	Gersdorffite	7	Pyrite
NiAbS	Ullmannite	7	Pyrite
$CoSe_2$	Hastite	7	Marcasite
$CoTe_2$	—	7	Brucite
NiS_2	Vaesite	8	Pyrite
$NiSe_2$	Penroseite	8	Pyrite
$NiTe_2$	Melonite	8	Brucite

[a] Ignoring minor structural distortions.

a ladder-like arrangement parallel to the *c*-axis; similar arrangements are found in loellingite and arsenopyrite but not in pyrite. FeS_2 appears to represent the marginal case in which energy differences between the pyrite and marcasite structures are very small, repulsion between cations and attraction between anion pairs being balanced.

The dichalcogenides, therefore, are a good example of the insight provided by a ligand field approach to understanding a family of sulfide minerals. Nickel (1970) used a similar approach in discussing bonding in the skutterudites ($(Co,Ni,Fe)As_{3-x}$), explaining observed magnetic data and rationalizing solid solution limits in terms of the *d*-electron configurations. However, as detailed below, the ligand field model for dichalcogenides has been criticized and alternative theories proposed to explain structural relationships.

QUALITATIVE MOLECULAR ORBITAL (MO) AND BAND MODELS

The molecular orbital (MO) theory approach to bonding in sulfides has been a particularly powerful one, given the degree of "covalence" exhibited by these materials. Both qualitative and quantitative MO models provide great insights into the small molecules and clusters important in the solution chemistry of sulfides (and, in some cases, such clusters interacting with surfaces). Although metal-sulfur clusters have obvious limitations for the description of crystalline solids, they have provided powerful ways of modeling certain properties and of modeling the behavior dominated by localized electrons (e.g., many types of spectra in the visible-UV and X-ray regions). Also, in terms of qualitative models, the familiar molecular orbital energy level diagram for a single metal-sulfur cluster forms the basis (through "overlap"

of large numbers of adjacent clusters) for the transition to a simple qualitative band theory (or "MO/band theory") model (and the so-called "one-electron" energy band scheme).

Pyrite and the related disulfides and dichalcogenides provide a good example with which to illustrate the MO and MO/band theory approach. An MO energy level diagram for pyrite based on Bither et al. (1968), Burns and Vaughan (1970) and Burns (1993) is shown in Figure 2. The tetrahedral coordination of the sulfur atoms in pyrite to three metals and another sulfur suggests involvement of 3*s* and 3*p* orbitals (sp^3 hybridized) in forming σ-bonds. One hybrid sp^3 orbital from each of the six sulfurs forms six σ-bonds with d^2sp^3 hybrid orbitals of the central transition metal. The d^2sp^3 hybrids consist of the two e_g orbitals ($d_{x^2-y^2}$ and d_{z^2}), the one 4*s* orbital and the three 4*p* orbitals. Bither et al. (1968) assumed that the three t_{2g} orbitals (d_{xy}, d_{yz}, d_{xz}) of the transition metal remain *nonbonding*. The energy separation between nonbonding t_{2g} and antibonding e_g^* orbitals is designated $\Delta_{cov\text{-}\sigma}$ and is analogous to the ligand field stabilization energy. Burns and Vaughan (1970) suggest that the paired electrons in the nonbonding t_{2g} orbitals may form π bonds with vacant t_{2g}-type 3*d* orbitals of the sulfur atoms. This would result in the increased energy separation between nonbonding t_{2g} and antibonding e_g^* levels shown in Figure 2, i.e., $\Delta_{cov\text{-}\pi} > \Delta_{cov\text{-}\sigma}$.

Overlapping of molecular orbitals between $Fe(S\text{-}S)_6$ "clusters" in an FeS_2 crystal would cause broadening into bands. The "one-electron" energy band scheme for pyrite shown in Figure 3a originates from this qualitative approach (after Bither et al. 1968; Goodenough 1972). The main bonding molecular orbitals now form the filled σ band and the corresponding antibonding orbitals the empty σ* band, constituting the main valence and conduction bands

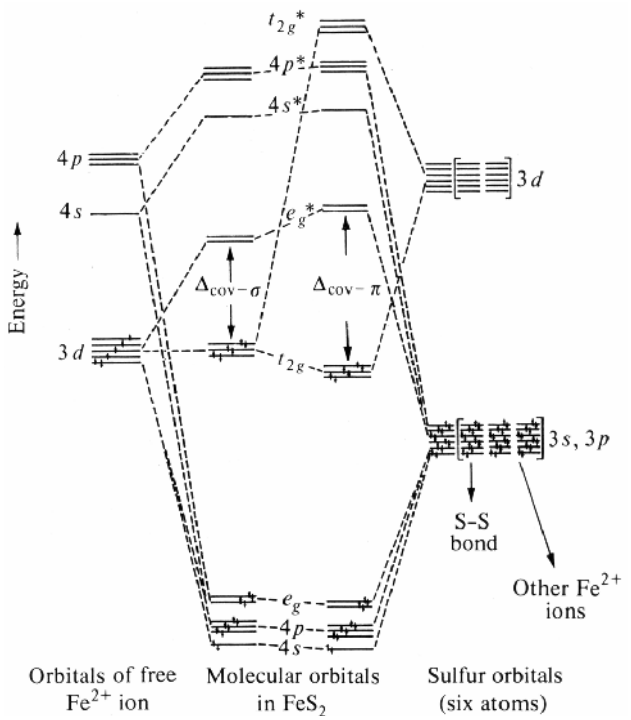

Figure 2. Molecular orbital energy level diagram for pyrite, FeS_2. (redrawn after Burns and Vaughan 1970).

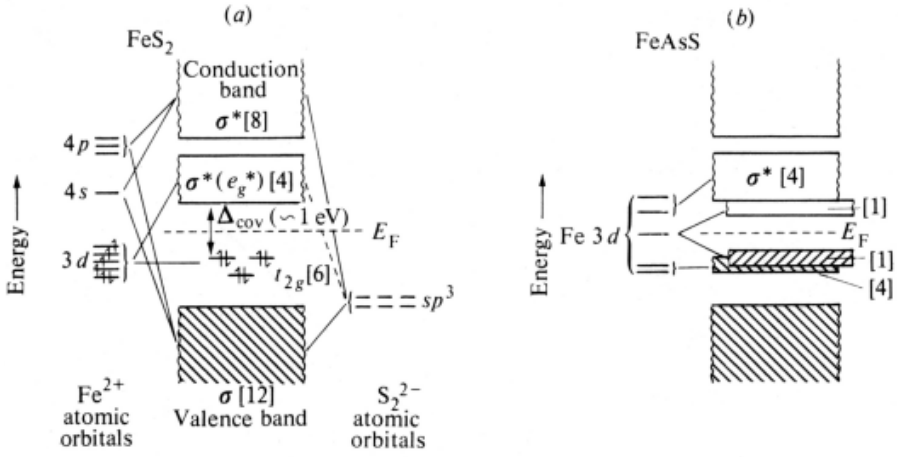

Figure 3. Schematic "one electron" energy band diagrams for: (a) pyrite (FeS_2) and (b) arsenopyrite (FeAsS). Numbers in square brackets refer to states per molecule; E_F = Fermi level; hatched bands are filled with electrons. (Redrawn after Bither et al. 1972; Goodenough 1972.)

respectively. The iron 3*d* orbitals then lie between these in energy, the t_{2g} orbitals being regarded as essentially localized on the cation but the e_g orbitals forming a band through overlap via sulfur intermediaries. Thus, conduction in pyrite would occur when electrons are excited into the band formed from e_g^* orbitals.

Using this approach to the electronic structures of the pyrite-, arsenopyrite- and loellingite-type disulfides, Goodenough (1972) criticized the ligand field model of Hulliger (1968) (the basis for the ligand field model described in the section above). Essential features of Goodenough's energy band model for FeAsS (and $CoAs_2$) are shown in Figure 3b. The splitting of the metal 3*d* orbital energy levels by the ligand field in the arsenopyrite structure differs markedly from that in regular octahedral coordination and is such as to raise the energy of the t_{2g}-type orbital which is parallel to the *c*-axis. The other t_{2g}-type orbitals remain nonbonding orbitals and form a filled narrow band (cf. the localized t_{2g} electrons in FeS_2); the e_g-type orbitals are the empty antibonding orbitals forming a conduction band. The unique t_{2g}-type orbital is split by a bonding interaction into a lower-energy filled band and higher-energy empty band. However, the important difference between this model and the ligand field model outlined above is that the interaction (and hence the structural deformation) is attributed to metal-anion bonding not metal-metal bonding. Goodenough (1972) argues that the arsenopyrite structure represents an expansion, not a contraction, of alternate metal-metal separations along the *c*-axis, and that electron density is concentrated in the regions of *greater* separation.

The pyrite and arsenopyrite disulfides serve to emphasize the difference between the localized electron approach of ligand field theory and the collective electron MO/band theory in describing the *d* orbitals in sulfides. Further illustrations can be provided by comparing the electronic structures of the pyrite-structured MnS_2 (hauerite) and NiS_2 (vaesite) with pyrite itself. In MnS_2, the 3*d* electrons are localized on the cation, partly because of the large intra-atomic stabilization energy gained by the high-spin d^5 configuration. Effectively, the five single *d*-electrons are more tightly bound. The intra-atomic exchange energy (Δ_{ex}) required to produce pairing of the *d*-electrons is a maximum value and can be represented as in the 3*d* orbital energy band diagram of Figure 4. Expressed another way, the *d* orbital energy levels are split into a spin-up (α) and spin-down (β) set. It is unnecessary to invoke such splitting to explain the properties of FeS_2 shown in Figure 4. The series of pyrite-structure

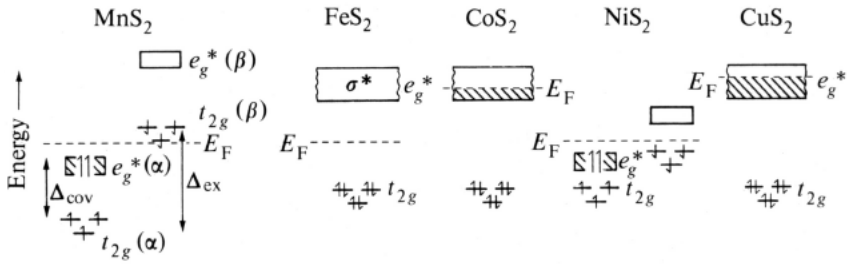

Figure 4. Schematic energy level diagram for the 3*d* orbitals in the pyrite-type disulfides (only 3*d* orbital energy levels are shown). The effects of intra-atomic exchange are shown in MnS_2 and NiS_2.

compounds FeS_2-CoS_2-NiS_2-CuS_2 sees successive addition of electrons into the e_g^* band and the progressive changes in properties outlined elsewhere in this volume (see, for example, Pearce et al. 2006). The energy band diagrams for just the 3*d* orbitals are shown in Figure 4 and accord with the metallic conductivity of CoS_2 and CuS_2, although in CoS_2 the e_g^* band is sufficiently narrow that ferromagnetism is observed at low temperatures. In NiS_2 the intra-atomic exchange energy again becomes important, splitting the energy levels into spin-up and spin-down states. The localized magnetism and semiconductivity of NiS_2 can be viewed as consequences of this interaction. The MO/band approach can, therefore, describe the complete range of properties exhibited by the pyrite-type disulfides, from the localized 3*d* electron behavior of MnS_2 to the broad band (metallic) delocalized 3*d* electron behavior of CuS_2.

The same MO/band theory approach has been used to describe the bonding in other major sulfide mineral groups, including the NiAs-type monosulfides, thiospinels, and the pentlandites. Some of these examples are discussed below (but see also Vaughan and Craig 1978, for further discussion of the earlier work).

QUANTITATIVE APPROACHES: ATOMISTIC COMPUTATION

One of the quantitative approaches that has been employed to model chemical bonding in minerals is the use of so-called *atomistic* calculations based on the Born Model of solids. Here, in a classical rather than quantum mechanical formalism, the atoms comprising the crystalline solid are regarded simply as ions, and the (non-directional) forces between them modeled using interatomic potentials. Short range interactions are generally modeled using a Buckingham potential:

$$U_{ij} = \sum_{ij} A_{ij} \exp\left[r_{ij}/\rho_{ij}\right] - C_{ij} r_{ij}^{-6} \tag{1}$$

where i and j are two ions with separation r, A and ρ are constants describing short range repulsion and C is a term that takes dispersion effects into account. Long range contributions from Coulombic interactions are also incorporated in these models in various ways. Also, rather than having to regard the ions involved purely as rigid spheres, the effects of the polarizability of the ion (and hence distortion of charge distribution in its environment in the crystal) can be incorporated, and additional potential terms added to account for the directionality of bonds. The actual potential parameters are most commonly derived by empirical fitting to accurately known experimental data, although an alternative approach is to use parameters derived *ab initio* using quantum mechanical methods. A full account of atomistic computational methods can be found in references such as Catlow (1997), and a good introduction for the mineralogist is provided by Gale (2001).

High quality atomistic calculations can be successfully used to model crystal structure, crystal morphology, energetics, lattice dynamics and properties such as elastic and dielectric constants. They have also been used to simulate the structure and stability of the surfaces of crystalline solids and to model defects, and behavior related to the presence of defects, such as diffusion. Of course, they provide no information on electronic structure or on properties (electrical, magnetic, optical, etc.) that can only be understood in terms of electronic structure.

Although atomistic methods have mainly been used to model materials such as oxides, silicates and carbonates, there have been successful applications to sulfides, despite the limited extent to which sulfides can be regarded simply as "ionic" solids. Wright and Jackson (1995) used this approach to simulate the structure and defect properties of ZnS. Their potentials reproduce the structure and elastic constants to within a few percent of the experimental values, and their calculations suggest that Zn diffusion in ZnS takes place via an interstitial mechanism, whereas S diffuses by way of vacancies in the lattice. Wright et al. (1998) went on to use the same potentials to simulate the structure and stability of sphalerite surfaces. Hamad et al. (2002) generated a new set of Zn-S and S-S potential parameters and used them to model both the sphalerite and wurtzite forms of ZnS. This work included modeling of the relaxed surface geometry of the sphalerite (110) surface and the $(10\bar{1}0)$ surface of wurtzite. Calculated surface energies were used to predict the most stable crystal morphologies of both dimorphs. In the case of sphalerite, this is a dodecahedron comprised of only the (110) surface and its equivalents; in wurtzite, it is a highly anisotropic cylindrical-like shape. Recently, new interatomic potentials have been presented by Wright and Gale (2004) and used to model the structures and stabilities of both sphalerite and wurtzite polytypes of ZnS and CdS. These potentials reproduce many of the properties of all four minerals to within a few percent of experimental values. In contrast to the majority of previous calculations, the relative stabilities of the cubic and hexagonal phases are correctly predicted, with the cubic form being more stable for ZnS and the hexagonal form for CdS. In $Zn_xCd_{1-x}S$ solid solutions, the transition from hexagonal to cubic is predicted to occur at $x = 0.6$.

More surprising than the success in using atomistic simulations to model particular properties of ZnS has been the work on pyrite and marcasite by Sithole et al. (2003). Here, interatomic potential parameters derived at simulated temperatures of 0 K and 300 K (referred to as P1 and P2, respectively) were used to predict structures and elastic properties as a function of pressure up to 44 GPa. Predicted pyrite structures were within 1% of those determined experimentally and the calculated bulk modulus was within 7%. As illustrated in Figure 5, the calculated equation of state (EOS) for pyrite gives good agreement with experimental data (such as that of Merkel et al. 2002). The calculations show that Fe-S bonds shorten more rapidly than S-S dimer bonds, and that marcasite shows very similar behavior to pyrite at high pressure. The vibrational spectrum of pyrite has also been modeled with some success using lattice dynamics atomistic simulations (Lutz and Zminscher 1996).

QUANTITATIVE APPROACHES: ELECTRONIC STRUCTURE CALCULATIONS

These days, the electronic structure of sulfide minerals is most commonly discussed from first-principles terms using a quantitative approach based on either molecular orbital theory or band theory. As noted above, this has largely to do with the continually improving efficiency and sophistication of electronic structure calculations. In the present view, we concern ourselves generally with the energies and spatial distribution of electronic states traveling throughout the solid. The electronic structure depends on all possible interactions between particles in the material. We approach the problem using the Schrödinger equation:

$$H\Psi = E\Psi \tag{2}$$

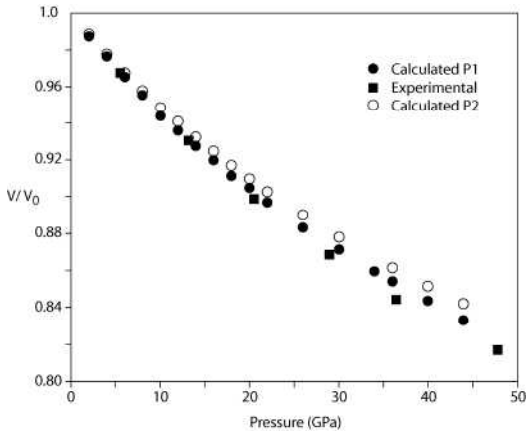

Figure 5. Atomistic calculation of the equation of state (EOS) of pyrite compared with experimental data (after Sithole et al 2003).

where H is the Hamiltonian operator, Ψ is the wavefunction, and E is the total energy of the system. A usual non-relativistic Hamiltonian is written:

$$H = H_e + H_{eN} + H_N \tag{3}$$

where the electron-electron interaction term is:

$$H_e = \sum_i -\frac{\hbar^2}{2m}\nabla_i^2 + \frac{1}{2}\sum_{i,j\neq}\frac{e^2}{|\mathbf{r}_i - \mathbf{r}_j|} \tag{4}$$

the nuclear-nuclear interaction term is:

$$H_N = \sum_I -\frac{\hbar^2}{2M_I}\nabla_I^2 + \frac{1}{2}\sum_{I,J\neq}\frac{Z_I Z_J e^2}{|\mathbf{R}_I - \mathbf{R}_J|} \tag{5}$$

and the electron-nuclear interaction term is:

$$H_{eN} = -\sum_{iI} Z_I \frac{e^2}{|\mathbf{R}_I - \mathbf{r}_i|} \tag{6}$$

where **r** and **R** are position vectors for electrons and nuclei, respectively, m and M are electron and nuclear masses, respectively, and Z is a nuclear charge.

In a first principles calculation one seeks a solution to the Schrödinger equation. To accomplish this requires many approximations. Some of the main ones relevant to this discussion are: (1) the Born-Oppenheimer approximation involving separation of electronic and nuclear motions; (2) the one-electron or mean-field approximation where each electron is treated as traveling on a periodic potential arising from the nuclear charges modified by the average potential contribution of all the other electrons, and (3) Koopmans' approximation, which allows one to impart physical significance (i.e., ionization potentials) to the one-electron eigenvalues by assuming electron removal does not affect the energies of other one-electron states. In general, other approximations are specific to the approach for implementing the calculation in a practical manner.

For example, the Hartree-Fock (HF) approach is an attempt to treat the many-body problem directly by keeping track of the coordinates of all the electrons. HF describes the wavefunction in terms of a single Slater determinant, a determinant of a matrix of one-electron "spin" orbitals. The interactions between the electrons are expressed as Coulomb

and exchange integrals. The task is to determine the lowest energy wavefunction for the entire system of interacting electrons, where a change in the spin orbital for one electron influences the behavior of other electrons due to coupling of the electronic motions. In HF, this is done by focusing on a single electron in a spin orbital interacting with the fixed field of nuclei and the fixed field of other electrons. But since the solution for one electron affects the remaining electrons, an iterative scheme called the self-consistent field (SCF) approach is used to find the overall solution. Electron exchange is a short range electron-electron interaction that excludes the possibility of electrons of like spin from occupying the same orbital (the Pauli exclusion principle). In HF this is a built-in property of the Slater determinant (antisymmetry). In the HF equations, the exchange term modifies electron-electron repulsion only for electrons of like spin. The effect is to spatially separate electrons of like spin in the calculation, which gives rise to a slight reduction in the total energy called the exchange energy. A strength of the HF approach is its exact expression for the electron exchange energy. However, the exchange interaction does not fully describe the tendency of electrons to avoid each other. The difference between the HF energy and the exact energy is the correlation energy. This deficiency leads to overbinding of electrons to nuclei, and consequently very poor prediction of bond energies and band gaps. The usefulness of the HF approach for understanding the electronic structure of "strongly correlated" systems such as sulfide minerals is very constrained.

Density functional theory (DFT) is a very different approach that does provide for a treatment of both electron exchange and correlation. The main idea of DFT is to replace the many-body electronic wavefunction with the electron density as the central quantity. An early implementation of DFT that was heavily used for solid-state electronic structure calculations was the multiple-scattering SCF X_α method. MS-SCF-X_α is a molecular orbital method wherein the one-electron Schrödinger equation is set up for a so-called "muffin-tin" approximation of the true potential, spherically symmetrical within spheres surrounding the various nuclei and constant in the region between the spheres. It uses a statistical approximation for exchange-correlation. This method was often successful for describing sulfide mineral electronic structure and is mentioned here because this early work is still useful, some of which is reviewed below (for more detailed information on this method and results for sulfides see Tossell and Vaughan 1992). Presently, however, it is typical for reports of sulfide mineral electronic structure to be based on so-called "modern" density functional theory (DFT) (Hohenberg and Kohn 1964; Kohn and Sham 1965). In this Kohn-Sham approach, the ground state wave function and energy are expressed as functionals of the electron density distribution. Exchange-correlation interaction is included in terms of an empirically parameterized functional. Incremental improvements to the accuracy of DFT historically have come in the form of improved exchange-correlation functionals. Early functionals were based on the limiting behavior of the uniform electron gas in what is known as the local density approximation (LDA). More refined exchange-correlation functionals include terms involving the spatial gradient of the charge density in what is known as the generalized gradient approximation (GGA). For sulfide minerals, the BLYP (Becke 1998; Lee et al. 1988), PW (Perdew and Wang 1992), and PBE (Perdew et al. 1996) GGA functionals are in common use. Becke's three parameter hybrid functional (B3LYP)(Becke 1993), based in part on a prescribed amount of HF exact exchange, is also in common use. While DFT performs better than HF, it is not without problems. Unlike HF, where electron interaction with itself is completely canceled, this self-interaction is only partially cancelled in typical DFT implementations (Perdew and Zunger 1981). Therefore, recently, improvements to DFT have been made by incorporating a self-interaction correction (Svane et al. 2004), by an amount that is sometimes empirical. Other recent improvements to DFT have been based on incorporating exact exchange (Stadele et al. 1999). These have led to substantially more accurate band gaps for instance.

DFT band structure calculations for crystals may be implemented using periodic boundary conditions at the unit cell edges. Basis sets (one-electron trial functions) could have the form of either local functions (typically Gaussians) such as in the Crystal code (Saunders et al. 2003)

or continuous (e.g., planewave) functions such as in the NWChem code (Apra et al. 2003). The solution is a set of wavefunctions and energy eigenvalues for each one-electron state. The one-electron wavefunctions are Bloch functions, which have the form of planewaves, modulated by a function whose periodicity is the same as that of the crystal lattice, as given by:

$$\psi_{\mathbf{k}}(\mathbf{r}) = e^{i\mathbf{k}\cdot\mathbf{r}} u_{\mathbf{k}}(\mathbf{r}) \tag{7}$$

where $\psi_{\mathbf{k}}(\mathbf{r})$ is the Bloch function, $u_{\mathbf{k}}(\mathbf{r})$ is the periodic function, $\mathbf{r}$ is a position in the unit cell, and $\mathbf{k}$ is the propagation vector. The energy level structure for these states consists of groupings (or bands) of allowed energy levels (where $\mathbf{k}$ is real), separated by energy gaps where no electronic states are allowed (where $\mathbf{k}$ is complex). The band structure is displayed as energy vs. $\mathbf{k}$, where $\mathbf{k}$ vectors are chosen along high symmetry directions in the Brillouin zone. The Fermi level (E_F) lies in the band gap between the occupied (valence) and unoccupied (conduction) bands, designating the energy at which the chemical potential of electrons is zero.

DFT works well for describing electrons in metallic or small band gap sulfide minerals where very strong interatomic interactions exist, such as covellite, millerite, and cattierite. The band structure calculations can provide useful insights into how atomic orbitals are combined into crystalline orbitals comprising bands. In many sulfide minerals, band energies are typically closely related to the energies of the free atom states. One example is where metal cations lead to partially filled *d*-bands, such as in many of the pyrite-type disulfide minerals where the cation is a first-row transition metal atom. In this case, band widths can be relatively narrow and band gaps are non-zero. Various methods are available for decomposing the wavefunction for the crystal in terms of the individual atomic wavefunctions (e.g., projected densities of states, crystal orbital overlap population analysis, etc.). This allows bands to be spoken of in terms of their atomic orbital character (e.g., *s*-*p* band, *d*-band, etc.). Close spacing and high degree of atomic orbital hybridization between the atoms is the basis for covalent bonding, which gives bands that are strongly mixed in their atomic orbital character. Hybridization is most significant for valence atomic orbitals, producing a mixed band which is smoothly varying across atom types in the crystal and allowing for electron delocalization.

Lastly, it is worth noting that most DFT studies of sulfide minerals so far have primarily been "static" calculations, intrinsically for a temperature of zero Kelvin. *Ab initio* molecular dynamics, particularly using the Car and Parrinello scheme (Car and Parrinello 1985) (CPMD) is beginning to be applied to sulfide minerals. In CPMD, the minimization of the total energy with respect to the total wavefunction and atomic coordinates is solved simultaneously and molecular dynamics is performed at only a slight increase in computational expense. A planewave basis set is used, often with pseudopotentials to mimic the scattering properties of core electrons and explicit description only of the valence electrons. CPMD is highly efficient quantum mechanical molecular dynamics at the DFT level of theory. It has provided a means to study sulfide mineral properties and reactions that depend on both the electronic and nuclear motion at temperatures of interest.

CHEMICAL BONDING AND ELECTRONIC STRUCTURE IN SOME MAJOR SULFIDE MINERALS AND GROUPS

Generalities

The development of quantitative bonding models for sulfide minerals has lagged behind the work in this field on oxides and silicates. This has been partly because of the more limited geological abundance and perceived importance of sulfides, but chiefly because of the challenge to modeling posed by the diversity of electronic structure types found in this mineral group. In what follows, our current knowledge of bonding in some major sulfide minerals and

groups is reviewed, noting the usefulness of both qualitative and quantitative cluster (MO) and periodic (band model) approaches. A number of more wide ranging computational studies of sulfides have been published in recent years, in addition to relevant material in the review volumes already mentioned, and these are discussed here.

Gibbs et al. (1999) calculated electron density distributions $\rho(\mathbf{r})$ for a large number of model sulfide molecules and their oxide equivalents, and applied the concepts developed by Bader and coworkers to characterizing the differences between sulfide and oxide bonds. Bader (1990, 1998) has argued that atomic interactions in "molecular" systems can be identified and characterized by the topological properties, the gradient, and the Laplacian $\nabla^2\rho(\mathbf{r})$ of their electron density distributions (e.g., Bader 1990, 1998). In their study, Gibbs et al. (1999) provide a quantitative demonstration that bonded interactions in sulfides are more directional for a given cation compared with oxides. They also show that the value of the electron density distribution at the bond critical point, and the length of the M-S bond, are reliable measures of a bonded interaction; the greater the accumulation of electron density at the bond critical point and shorter the bond, the greater the covalent interaction. Laplacian maps of the electron density distribution for sulfur-containing molecules in comparison with the same molecules containing oxygen are illustrated in Figure 6. Here it can be seen that the valence shell charge concentration (VSCC) of the sulfide anion (dashed line contours) is highly polarized and extends into the internuclear region of the M-S bonds. In contrast, the corresponding oxide anion tends to be less polarized and more locally concentrated in the vicinity of its valence shell.

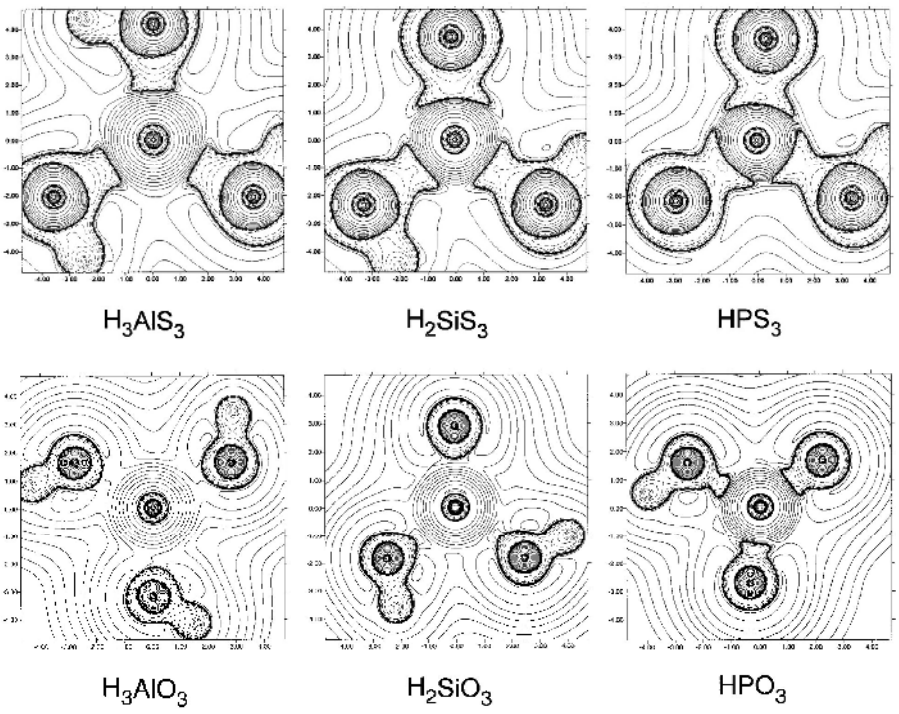

Figure 6. Laplacian maps of the electron density distribution calculated for equivalent oxygen and sulfur containing molecules. A metal cation is located at the center of each molecule and H atoms are attached to the oxide or sulfide anions to achieve electrical neutrality. (Reproduced from Gibbs et al. 1999; see this reference for further details.)

Similarly, analyses of electron density distributions have given insights into how various types of bonded interactions present in sulfides can be related to electronic properties such as electrical conductivity, a macroscopic observable. For example, electron density distributions were computed and analyzed for the bonded interactions comprising the nickel sulfide minerals millerite, vaesite, heazlewoodite, and also Ni metal (Gibbs et al. 2005). These analyses identified Ni-Ni bond paths restricted to isolated Ni_3S_9 clusters in millerite (a S p – Ni d charge transfer conductor), and were found to form contiguous highly branched networks in heazlewoodite (a Ni 3d metallic conductor). No Ni-Ni bond paths were found in vaesite (an insulator). Electron transport in Ni metal and heazlewoodite was pictured as occurring along the Ni-Ni bond paths, which behave as networks of atomic-size wires that radiate in a contiguous circuit throughout the two structures. In contrast, electron transport in millerite is pictured as involving a cooperative hopping of the d-electrons from the Ni_3 rings comprising Ni_3S_9 clusters to Ni_3 rings in adjacent clusters via the p orbitals on the interconnecting S atoms.

A number of theoretical studies have been aimed at calculating the electronic structures of a series or large group of sulfides. In earlier work, for example, Harris (1982) used cluster calculations (MS_6^{n-} clusters) to study the electronic structures of first and second row transition metal sulfides, calculating trends in energy levels and charge distributions, and concluding that the bonding in second row transition metal sulfides is more covalent than in the first row due to increased metal-sulfur d-$p\pi$ interactions.

Certain first row transition metal sulfides have also featured in systematic studies aimed at exploring different theoretical approaches or the subtleties of electrical or magnetic properties (Bauschlicher and Maitre 1995; Saitoh et al. 1995; Rohrbach et al. 2003). In a series of calculations using DFT, Raybaud et al. (1997a,b) investigated the structural and cohesive properties and the electronic structures of more than thirty transition metal sulfides, including the monosulfides of V, Cr, Mn, Fe, Co, Ni, Pd and Pt; disulfides of Mn, Fe, Co, Ni, Mo, Ru, Pd, Re, Os, Ir, and more unusual phases such as Co_9S_8 and Ni_3S_2. Although initial calculations using the LDA tended to overestimate the strength of bonding, using GGA the structures and cohesive energies were more accurately predicted. Calculated cohesive energies are shown in Table 2. The general conclusions regarding electronic structure were that it is determined by short range interactions in the S 3p – metal d band complex, with the ligand field splitting of the metal d states by the surrounding S atoms determining the structure of the d band. The authors were able to predict electrical properties, and to comment on factors influencing the catalytic activity of the various transition metal sulfides studied. Correlations between catalytic activity and both metal-sulfur bond strength and the character of the highest occupied states (so-called "frontier orbitals") were noted. This formidable series of calculations provides a good illustration of how much can now be achieved using *ab initio* computation to study sulfide minerals. In addition, Hobbs and Hafner (1999) have extended the work of Raybaud et al. (1997a,b) by using the DFT approach to calculate the magnetic properties of key transition metal sulfides (CrS, MnS, FeS, CoS, NiS, MnS_2, FeS_2, CoS_2, NiS_2).

Galena (PbS)

As noted elsewhere in this volume (Mackovicky 2006; Pearce et al. 2006; Wincott and Vaughan 2006), the rocksalt structure PbS is a small bandgap (~ 0.4 eV) intrinsic semiconductor, although natural samples may show either n- or p-type behavior dependant on the presence of defects and impurities. Both bulk and surface electronic structure and properties have been the subject of numerous spectroscopic and computational studies (surface studies are discussed in this volume by Rosso and Vaughan 2006a,b). Amongst experimental data available are optical reflectance and transmittance spectra (Cardona and Greenaway 1964; Schoolar and Dixon 1965), detailed X-ray and UV photoemission and inverse photoemission spectra (McFeely et al. 1973; Grandke et al. 1978; Santoni et al. 1992; Ollonqvist et al. 1995; Schedin et al. 1997; Leiro et al. 1998; Muscat and Klauber 2001), Auger electron spectra

Table 2. Cohesive energies of the transition-metal sulfides (in eV/atom).

Structure	E_{exp}	E_{GGA}	E_{GGA}/E_{exp}	E_{LDA}/E_{exp}
3d				
VS	5.61	5.02	0.90	1.12
Cr_2S_3	4.79	3.81	0.80	1.06
CrS	—	4.09	—	—
MnS	4.03	4.03	1.00	1.12
FeS(NiAs)	4.14	4.42(6)	1.07	—
FeS (troilite)	—	4.43(5)	—	—
FeS_2 (pyrite)	3.92	4.29	1.08	—
FeS_2 (marcasite)	3.92	4.31	1.10	—
Co_9S_8	4.23	4.91	1.15	1.44
CoS	4.10	4.68	1.14	—
Ni_3S_2	4.30	4.54	1.06	—
NiS (millerite)	4.12	4.39	1.07	—
NiS (NiAs)	—	4.32	—	—
NiS_2	—	4.02	—	—
4d				
NbS	—	6.16	—	—
NbS_2	5.68	5.54	0.98	—
MoS_2	5.18	5.11	0.99	1.21
RuS_2	4.88	5.05	1.03	1.28
Rh_2S_3	4.61	4.84	1.05	1.29
PdS	3.80	3.76	0.99	1.26
PdS_2	—	3.60	—	—
5d				
TaS_2	5.87	6.04	1.03	—
WS_2	5.78	1.00	1.00	1.20
ReS_2	5.23	5.35	1.02	—
OsS_2	5.19	5.34	1.03	1.26
$Ir2S_3$	5.06	5.37	1.06	—
IrS_2	4.77	5.07	1.06	—
PtS	4.83	4.69	0.97	1.20

(Tossell and Vaughan 1987), and a range of X-ray emission (Sugiura et al. 1997) and X-ray absorption spectra (von Oertzen et al. 2005). These spectroscopic studies have been reviewed elsewhere in this volume (Wincott and Vaughan 2006).

A wide variety of cluster (MO) and periodic (band structure) computational approaches have been applied to galena (Tung and Cohen 1969; Rabii and Lasseter 1974; Hemstreet 1975; Tossell and Vaughan 1987, 1992; Mian et al. 1996; Gurin 1998; Gerson and Bredow 2000; Satta et al. 2000; Muscat and Klauber 2001; Ma et al. 2004; Zeng et al. 2005). As noted by Rosso (2001), accurate computation of the electronic structure of galena is more difficult than might first appear because proper treatment of the heavy element Pb requires dealing with relativistic effects, and an all-electron treatment has to include the *f* electrons. Despite these complications, the computed values for band energies, band widths and densities of states of the valence band are in excellent agreement with experiments. Wincott and Vaughan (2006; this volume) illustrate how earlier cluster and band structure calculations inform interpretation of photoemission and X-ray emission and absorption spectra of galena. The composition of the valence region is illustrated in Figure 7 using results of a recent calculation of the density

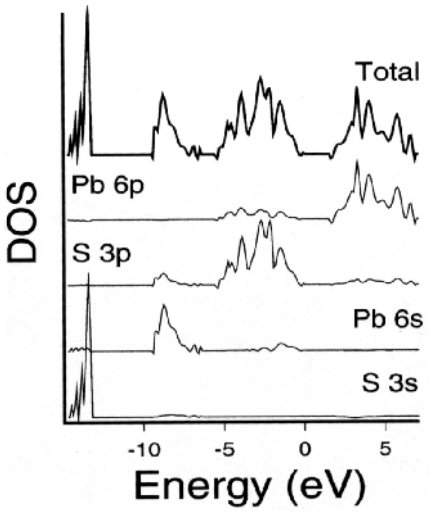

Figure 7. Calculated total and projected densities of states (DOS) for galena using data from Becker and Rosso (2001). The Fermi level (zero on the energy scale) is arbitrarily located at the valence band edge. The top of the valence band is seen here as being comprised of predominantly S 3*p* states and the bottom of the conduction band as comprised of predominantly Pb 6*p* states. (Reproduced from Rosso 2001.)

of states (see Rosso 2001; Becker and Rosso 2001). As can be seen, the conduction band is dominated by Pb 6*p* states with a minor admixture of S 3*p* states. The top of the valence band consists of non-bonding S 3*p* states, overlying a Pb 6*s* – S 3*p* bonding band. It is interesting to note that calculation of electron density maps and of other indictors of the nature of bonding, such as orbital overlaps, show that the bonding in galena can be described as ionic with minor covalent character (Mian et al. 1996).

Sphalerite and related sulfides (ZnS, Zn(Fe)S, CdS, HgS, $CuFeS_2$)

The cubic (sphalerite) and hexagonal (wurtzite) forms of ZnS are classic crystal structure types, both containing Zn and S in regular tetrahedral coordination. Both are also diamagnetic semiconductors with large band gaps (sphalerite ~ 3.6 eV; see Pearce et al. 2006, this volume for details). Sphalerite and wurtzite, along with the two isostructural CdS species (hawleyite and greenockite) have also been the subject of numerous experimental and computational studies of bonding and electronic structure, partly because of their interest to solid state physicists. This includes investigations of sphalerite using X-ray photoelectron and X-ray emission spectroscopies (e.g., Ley et al. 1974; Sugiura et al. 1974; Domashevskaya et al. 1976; Sugiura 1994; Laihia et al. 1996, 1998) and X-ray absorption spectroscopies (Li et al. 1994a,c; von Oertzen et al. 2005) reviewed elsewhere in this volume (Wincott and Vaughan 2006).

Calculations have been performed on ZnS using both MO cluster methods (e.g., Tossell 1977) and a large variety of band structure methods (e.g., Stukel et al. 1969; Pantelides and Harrison 1975; Faberovich et al. 1980; Bernard and Zunger 1987; Martins et al. 1991; Schroer et al. 1993; Edelbro et al. 2003). As noted above, ZnS has also been successfully studied using atomistic methods. The calculations of Edelbro et al. (2003) using an DFT approach are typical of the level of detail now attainable and in Figure 8 are shown the band structure (Fig. 8a) and the calculated density of states (DOS) with Zn and S contributions (Fig. 8b) obtained by these authors for sphalerite ZnS. As can be seen from Figure 8b, the valence band is calculated to be a mixture of Zn and S orbitals and to lie in the interval from −5.2 to 0 eV, in good agreement with experiment (such as the XPS data of Ley et al. 1974). Below these levels (at −6.5 eV) are the Zn 3*d* bands which are around 3 eV higher in energy than determined by experiment. The band at −11.7 to −12.9 eV comprises the S 3*s* electrons according to the calculations. The calculated band gap is somewhat underestimated compared with experiment

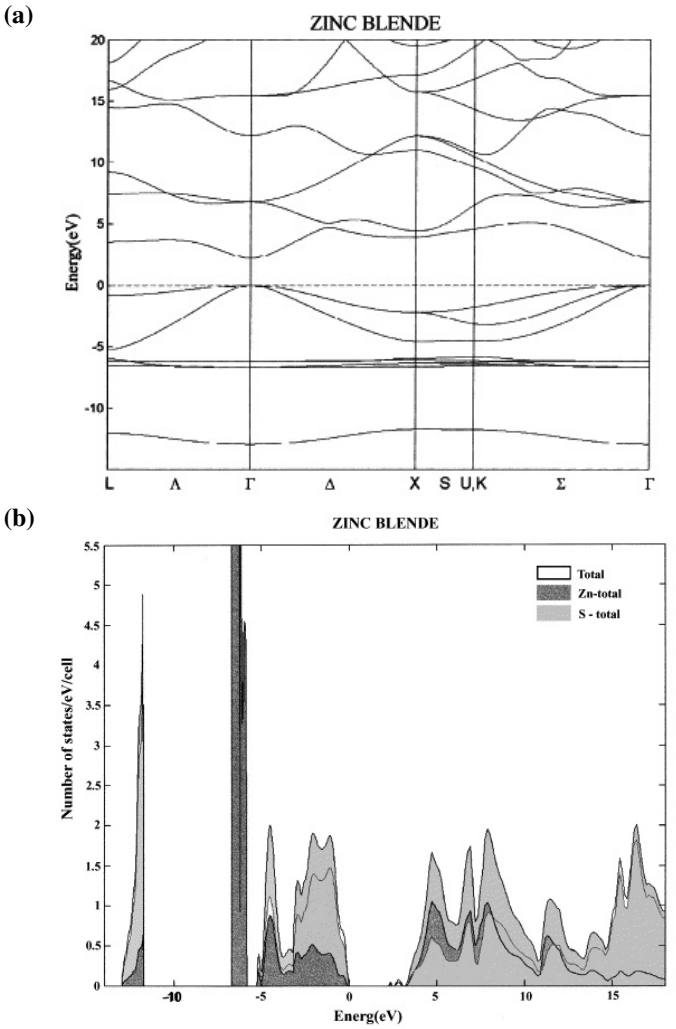

Figure 8. The electronic structure of ZnS (sphalerite): (a) calculated band structure with the zero of energy set at the highest occupied state; (b) the calculated density of states (DOS) showing the Zn and S contributions. [Used with permission of Elsevier, from Edelbro et al. (2003), *Applied Surface Science*, Vol. 206, Figs. 7 and 8, pp. 306 and 307.]

(2.23 eV vs. 3.6 eV), a well known problem with DFT calculations. Both these calculations and earlier studies aid in interpretation of the large amount of available experimental data, and show that the Zn 3*d* orbitals in sphalerite are non-bonding and located below the valence band, which has strong bonding orbital character.

In a study using MO cluster calculations applied to MS_4^{6-} tetrahedral units (using the MS-SCF-X_α method), Tossell and Vaughan (1981) were able to compare ZnS, CdS and HgS. As discussed elsewhere in this volume (Wincott and Vaughan 2006), the calculations on the ZnS_4^{6-} cluster can be used to interpret XPS and XES data for sphalerite, the generally good agreement between experiment and theory providing support for these models (which are applicable to both sphalerite and wurtzite structure types). As seen in Figure 9, the calculations suggest an overall

similarity in the electronic structure of the valence region in ZnS, CdS and HgS, with S 3*p* non-bonding orbitals at the top of the valence band, below them the main metal-sulfur bonding orbitals, then non-bonding metal 3*d* orbitals and at around 12 eV below the Fermi level, the S 3*s* non-bonding orbitals. The order of molecular orbitals is the same in each case, but there are significant differences, notably the trend towards decreasing stabilization of the main metal-sulfur bonding orbitals moving across the series ZnS-CdS-HgS. In Figure 9, for comparison, a calculation is also shown of a HgS_2^{2-} linear cluster, the basic unit found in the cinnabar form of HgS.

The well known substitution of Fe^{2+} for Zn in the ZnS structure has also been modeled using MO cluster calculations (Vaughan et al. 1974), in particular to calculate the optical absorption spectra of Fe-doped sphalerite (see Wincott and Vaughan 2006; this volume, for a figure showing this spectrum). The calculated and experimental absorption features are given in Table 3 and generally show good agreement; these data also demonstrate the importance of spin polarization due to the four unpaired 3*d* electrons on the Fe^{2+} cation, which splits the MO energy levels into spin-up and spin-down groups (see discussion in earlier section of this chapter). These calculations used a transition-state (TS) procedure which takes into account relaxation effects associated with electron transitions. Other transition metals (Ti, Mn, Co, Ni) can substitute for the Zn in ZnS, and the electronic structures of these dopants (as well as Fe) have also been studied using X-ray absorption spectroscopy (XANES) by a number of researchers (Lawniczak-Jablonska et al. 1996; Pattrick et al. 1998; Perez-Dieste et al. 2004).

Chalcopyrite ($CuFeS_2$) has a sphalerite-type structure, and is one of the relatively few ternary sulfides to be the subject of detailed studies of its electronic structure. Tossell et al.

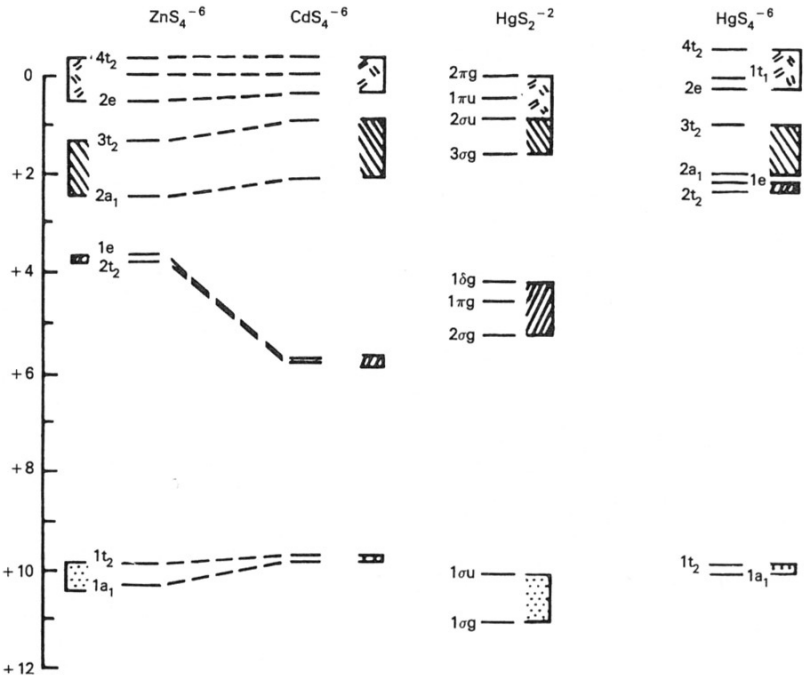

Figure 9. Energy level diagrams derived from cluster calculations (using the Multiple Scattering X_α method) on tetrahedral ZnS_4^{6-}, CdS_4^{6-}, HgS_4^{6-} clusters and the linear HgS_2^{2-} cluster. The makeup of particular MO energy levels in terms of atomic orbital character are shown by the boxes on the diagram. (After Tossell and Vaughan 1981.)

Table 3. Experimental and calculated optical spectra for the FeS_4^{6-} unit.
Transition energies, ΔE, are all in cm^{-1}.

Type of transition	Assignment	Calc. ΔE (TS)	Experimental ΔE
Spin-allowed *d*-*d*	$3e\downarrow \rightarrow 10t_2\downarrow$	2194	3850, 3500, 2950, 3700, 2850
Spin-forbidden	$10t_2\uparrow \rightarrow 3e\downarrow$	13,149	12,120, 13,000
Spin-flip (very weak)	$10t_2\uparrow \rightarrow 10t_2\downarrow$	14,279	14,500
	$3e\uparrow \rightarrow 3e\downarrow$	17,586	16,950
	$3e\uparrow \rightarrow 10t_2\downarrow$	18,586	19,600
Ligand-metal charge transfer	$2t_1\downarrow \rightarrow 3e\downarrow$	14,279	14,500
	$2t_1\downarrow \rightarrow 10t_2\downarrow$	13,100	
	$9t_2\downarrow \rightarrow 3e\downarrow$	17,586	16,950
	$9t_2\downarrow \rightarrow 10t_2\downarrow$	19,764	19,600

Source: After Vaughan et al. 1974, who provide details of the experimental data.

(1982) reported a fairly complete series of XES and XPS spectra, and used the results of MO calculations on CuS_4^{7-} and FeS_4^{5-} clusters to assign the features in these spectra. Mikhlin et al. (2005) studied the X-ray absorption (XANES) spectra of Fe, Cu and S (L-edges) in chalcopyrite and used a qualitative molecular orbital approach to interpret their data. Edelbro et al. (2003), following on from earlier band structure calculations (e.g., Hamajima et al. 1981), used an *ab initio* DFT approach to calculate the band structure of chalcopyrite, but their calculation predicted metallic conductivity, contrary to experimental findings. Lavrentyev et al. (2004) compared a combination of their own and other workers XES, XAS and XPS spectra for chalcopyrite with their calculated density of states using a cluster model. In Figure 10, a comparison of theoretical and experimental data from their study is shown. These data suggest that the main peak maximum (B) in the XPS arises from the copper *d*-electrons which, together with the *d* states of iron, also produce the shoulder A in the XPS. The shoulder C is attributed to Cu and Fe *d* states and a substantial contribution from sulfur *p* states. It is noteworthy that the 3*d* electrons of Cu appear to participate in bonding in this system, even though spectroscopic and magnetic evidence clearly shows that Cu is monovalent with a nominally filled 3*d* shell (see Pearce et al. 2006, Wincott and Vaughan 2006; both in this volume). Fujisawa et al. (1994), in reporting a series of detailed spectroscopic studies of $CuFeS_2$, state that the Cu 2*p* core XPS spectrum reveals a mixing of the d^9 ("Cu^{2+}") configuration into the formally monovalent Cu and interpret this as due to Cu 3*d*-Fe 3*d* hybridization mediated by the S 3*sp* valence states. There is further discussion of the electronic structure of chalcopyrite, particularly in the context of surface structure, in a later chapter of this volume (Rosso and Vaughan 2006b).

Transition metal monosulfides (FeS, $Fe_{1-x}S$, CoS, NiS)

The monosulfides FeS, CoS and NiS have the nickel arsenide structure at elevated temperatures but undergo distortion, structural transformation or breakdown on cooling (see Makovicky 2006; Fleet 2006, both in this volume). In the case of FeS, troilite (stable below 140ºC) is a distorted form of the NiAs structure in which triangular clusters of iron atoms form in the basal plane. There is also the $Fe_{1-x}S$ omission solid solution of the pyrrhotites, with its complex series of vacancy ordered superstructures, the most important of which is that of monoclinic pyrrhotite (Fe_7S_8). CoS undergoes dissociation forming cobalt pentlandite (Co_9S_8; see the separate section below) and NiS transforms to the millerite structure (see below).

As discussed, in part, elsewhere in this volume (Wincott and Vaughan 2006), a wide variety of spectra of these monosulfides have been studied. This includes S K_β and S K_α X-ray

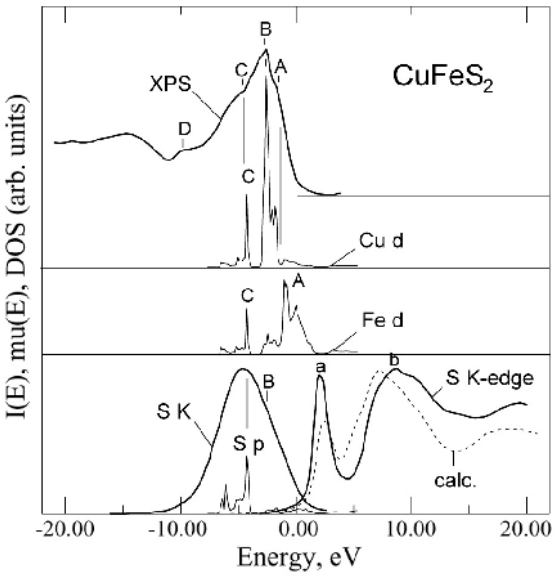

Figure 10. Comparison of experimental and theoretical data for chalcopyrite ($CuFeS_2$): Experimental XPS and S K_β emission spectra from Tossell et al. (1983); experimental S K absorption spectrum from Petiau et al. (1988); calculated densities of states for Cu 3*d*, Fe 3*d* and S 3*p* electron states (cluster calculation, Lavrentyev et al. 2004). [Used with permission of Elsevier, from Lavrentyev et al. (2004), *J. Electron Spectroscopy and Related Phenomenon*, Vol. 137-140, Fig. 4, p. 497.]

emission spectra (Sugiura et al. 1974; Marusak and Tongson 1979), Fe K_β X-ray emission spectra (Reuff et al. 1999; Gamblin and Urch 2001), XPS and UPS (Gopalakrishnan et al. 1979; Krishnakumar et al. 2002; Skinner et al. 2004), sulfur K and $L_{2,3}$ XANES and other XAS (Womes et al. 1997; Zajdel et al. 1999; Soldatov et al. 2004; Lavrentyev et al. 2004). The discussions of electronic structure have ranged from qualitative MO/band models based on observed properties (Goodenough 1967; Wilson 1972) to cluster calculations (e.g., Tossell 1977; Soldatov et al. 2004; Lavrentyev et al. 2004) and band structure calculations (Raybaud et al. 1997a,b; Krishnakumar et al. 2002).

The NiAs structure forms of FeS, CoS and NiS have been the subject of both experimental and computational studies. (Although high temperature forms, they can be retained at room temperature by quenching). Raybaud et al. (1997a) for example, using DFT band structure calculations, were able to make quite accurate predictions of the equilibrium crystal structures and of structural parameters such as cell volume and *c*:*a* axial ratios. In the companion paper, Raybaud et al. (1997b) the same computational approaches were used to model the electronic structures of the monosulfides and in Figure 11 shown their calculated electronic densities of states for FeS, CoS and NiS. Here the total densities of states (DOS) are shown and the *s*, *p* and *d* partial DOS for each phase. The bands can be arranged into four distinct groups: (1) S 3*s* at ~ −15 to −14 eV, (2) S 3*p* at ~ −8 to −3 eV overlapping with (3) the transition metal 3*d* bands around the Fermi level, and (4) the conduction band at > 4 eV made up from transition metal 4*s*, *p* and sulfur 3*d* states. The same authors also studied the low temperature forms, troilite, millerite and Co_9S_8 using the same computational methods. In comparison with the NiAs form, they found slight broadening of all the bands and increased S 3*p* – Fe 3*d* overlap in the case of troilite. They attribute the stabilization of the troilite phase over the NiAs-type to an increase in the binding energies of some of the Fe 3*d* (e_g) states associated with the closer Fe-Fe coordination. The

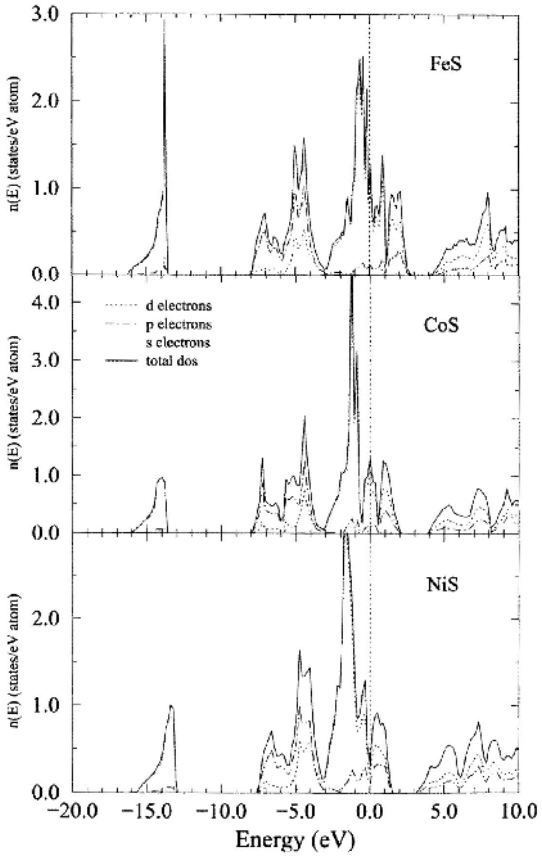

Figure 11. Calculated densities of states of the NiAs-structure FeS, CoS and NiS; solid line: total density of states; dotted, dashed and chain lines are *s*, *p* and *d* partial densities of states. [Used with permission of IOP Publishing Limited, from Raybaud et al. (1997), *J. Phys. Condens. Matter*, Vol. 9, Fig. 13, p. 11125.]

energetic stabilization of the millerite structure was similarly attributed to a slight shift to lower energies of certain Ni 3*d* (t_{2g}) states arising from the metal-metal interactions in the structure.

In considering other studies of the monosulfides, the results of calculations on an FeS_6^{10-} cluster (octahedrally coordinated high-spin Fe^{2+}; Tossell 1977) are presented and discussed elsewhere in this volume (Wincott and Vaughan 2006; see their Fig. 16), as is the simple band model for pyrrhotite based on these calculations and proposed by Sakkopoulos et al. (1984). Such a model is also used in the interpretation of spectroscopic data for a reacted pyrrhotite surface (Mikhlin et al. 1998) as discussed by Rosso and Vaughan (2006b, this volume; see their Fig. 33). Soldatov et al. (2004) used calculations on small clusters (19-37 atoms) employing a multiple scattering approach to compare with the results of their experiments recording the sulfur K and $L_{2,3}$ X-ray absorption near-edge structure (XANES) spectra of FeS, CoS and NiS. As can be seen from Figure 12 the agreement between experiment and theory was good in these studies. The electronic structures of the monosulfides were discussed on the basis of the calculations, with conclusions similar to those discussed above from the work of Raybaud et al. (1997b). For example, a systematic decrease in the separation between the sulfur 3*p* and the transition metal 3*d* bands in the series FeS-CoS-NiS (separations estimated at 3.52 eV (FeS),

3.50 eV (CoS) and 2.9 eV (NiS) by Soldatov et al. 2004) is regarded as a measure of increasing covalency across the series.

As noted above, NiS transforms on cooling below ~379 °C from the NiAs-type structure to the unique millerite structure in which nickel is in a NiS_5 square pyramidal coordination and sulfur is also in five-fold coordination (see Makovicky 2006; this volume). Millerite, with its very short metal-metal distances (~2.5 Å) has attracted interest as regards its electronic structure, in addition to that discussed above. Goodenough (1997) notes the metallic behavior and Pauli paramagnetism of millerite at room temperature, and the occurrence of another transition (T_N) at 264 K, below which millerite is a semimetallic antiferromagnet. Ikoma et al. (1995) and others have performed XPS experiments below this temperature (at 130 K). As discussed by Goodenough (1997), this must involve a transition from itinerant to more localized electron behavior. This transition is likely to be highly pressure dependant; indeed, millerite has been shown experimentally to be highly compressible compared with the NiAs-structure form (Sowa et al. 2004).

Krishnakumar et al. (2002) studied the electronic structure of millerite using XPS and UPS measurements and (DFT) band structure calculations (using the LMTO method and atomic sphere approximation). It was also found necessary to perform cluster calculations (using an NiS_5 cluster) that included electron correlation effects in order to model certain spectral features. Figure 13 shows the experimental valence band XPS spectrum from this work, along

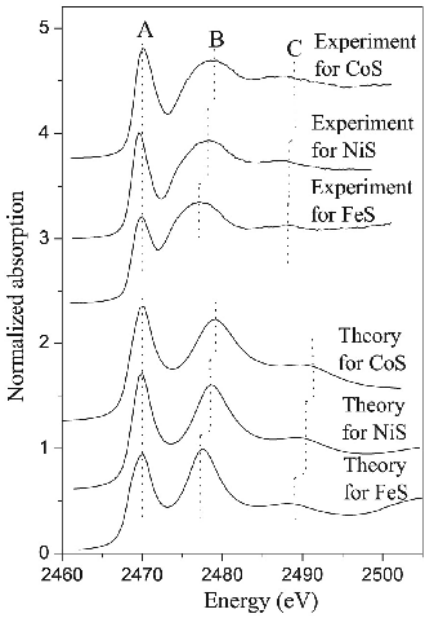

Figure 12. Comparison of experimental S K XANES spectra for FeS, CoS and NiS with theoretical spectra calculated using a cluster method. [Used with permission by IOP Publishing Ltd., from Soldatov et al. (2004), *J. Phys. Cond. Matt*, Vol. 16, Fig. 3, p. 7551.]

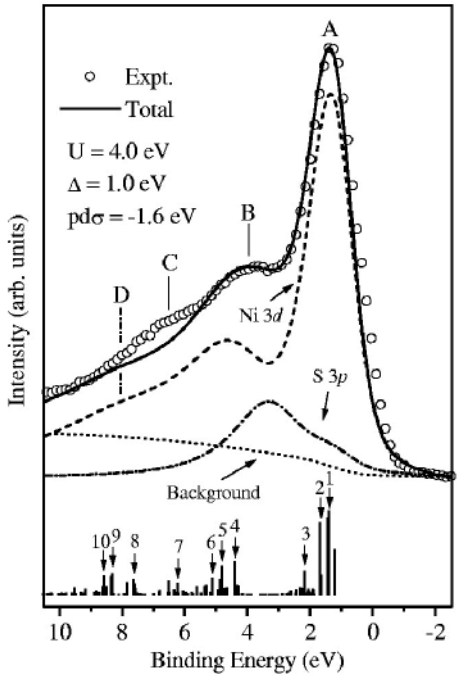

Figure 13. Experimental valence band XPS data (open circles) for millerite (NiS), along with the calculated spectrum (solid line) and the calculated Ni 3*d* and S 3*p* contributions and final states of the cluster calculation. [Reprinted with permission from Krishnakumar et al. (2002), *Phys. Rev. B*, Vol. 66, Fig. 5, p. 115105-5. © 2002 American Physical Society.]

with the calculated XPS spectrum and contributions to this spectrum from the Ni 3*d* and S 2*p* components. The detailed analysis of electronic structure provided by Krishnakumar et al. (2002) was summarized by them in describing millerite as a "highly covalent *pd* metal."

Pyrite and the related disulfides (FeS_2, CoS_2, NiS_2, CuS_2, FeAsS, $FeAs_2$)

Pyrite, with its low-spin Fe^{2+} octahedrally coordinated to S atoms in their dianion pairs, has been exhaustively studied experimentally and computationally. Much of the experimental evidence relevant to understanding its electronic structure is described elsewhere in this volume (Pearce et al. 2006; Wincott and Vaughan 2006). The data, which commonly extends to the isostructural MS_2 phases (where *M* is Co, Ni, Cu, and sometimes Zn) include optical reflectance spectra (Bither et al. 1968; Schlegel and Wachter 1976; Suga et al. 1983; Sato 1984; Ferrer et al. 1990; Huang et al 1993), photoemission spectra (Li et al. 1974; Ohsawa et al. 1974; van der Heide et al. 1980; Folmer et al. 1988; Fujimori et al. 1996; Bocquet et al. 1996) and X-ray emission and absorption spectra (Sugiura et al. 1976; Matsukawa et al. 1978; Mosselmans et al. 1995; Charnock et al. 1996; Lavrentyev et al. 2004; Prince et al. 2005).

A detailed discussion of qualitative MO and band models for pyrite and the isostructural Co, Ni and Cu disulfides has been presented earlier in this chapter. A large number of *ab initio* cluster and periodic calculations have been used to elucidate the electronic structure of these materials (Li et al. 1974; Tossell 1977; Bullett 1982; Folkerts et al. 1987; Temmerman et al. 1993; Fujimori et al. 1996; Raybaud et al. 1997; Eyert et al. 1998; Rosso et al. 1999; Gerson and Bredow 2000; Muscat et al. 2002; Edelbro et al. 2003). These calculations are generally in agreement with the each other and with the qualitative MO/band models for pyrite outlined above and illustrated in Figures 3a and 4. The pyrite band structure and total and partial densities of states from an LDA calculation of Eyert et al. (1998) are also illustrated here, in Figure 14. Thus, the top of the valence region is comprised of a narrow band of non-bonding Fe 3*d* t_{2g} electron states which lies a little above the main bonding band comprised of mixed S 3*p* and Fe 3*d* states (more specifically σ, π and π^* S_2^{2-} 3*p* states and e_g Fe 3*d* states). The high degree of mixing found here between cation and anion states is indicative of the strongly covalent bonding interactions in pyrite. As regards the bottom of the conduction band, both the qualitative models and most computational studies attribute it to a mixed S 3*p* – Fe 3*d* band composed of σ^* S 3*p* and e_g^* Fe 3*d* orbitals. However, in their calculation, Eyert et al. (1998) suggested that the bottom of the conduction band comprises exclusively S 3*p* states, this being attributed to a larger splitting of S 3*p* states arising from strong S-S σ interaction. This study also found a weak π-bonding component between the Fe 3*d* t_{2g} and S 3*p* orbitals supporting an earlier proposal by Burns and Vaughan (1970) that the t_{2g} states are not completely non-bonding.

The band gap which separates the top of the valence band from the bottom of the conduction band in this semiconducting sulfide, and which has a well established experimental value of 0.9-0.95 eV, is not well reproduced computationally. Typically the value is underestimated (e.g., a calculated value of 0.6 eV; Raybaud et al. 1997) although Eyert et al. (1998) predicted a value of 0.9 eV in what is undoubtedly a fortuitous result. In a detailed evaluation of different computational approaches to the electronic properties of pyrite, Muscat et al. (2002) attribute the discrepancy between experimental and computational values of the band gap to large deviations from stoichiometry in this mineral. However, there is no evidence for non-stoichiometry in pyrite on the scale proposed by them, and these discrepancies are more likely due to well known failings of the present levels of theory used to perform the calculations, as described above.

The series of pyrite-structure disulfides FeS_2-CoS_2 (cattierite)-NiS_2 (vaesite)-CuS_2-ZnS_2 show interesting variations in electrical and magnetic properties (Pearce et al. 2006, this volume) and have been extensively studied experimentally and using various computational methods. Most of the references to experimental studies cited at the beginning of this section include work on these other pyrite-structure phases. Qualitative models of electronic structure

for these phases are also outlined earlier in this chapter (see also Fig. 4). Elsewhere in this volume (Rosso and Vaughan 2006b) there is also some discussion of the electronic structure of the pyrite-structure RuS_2 (laurite), noting that its band structure is very similar to that of pyrite and describing, in some detail, the electronic structures of the (100), (111) and (210) surfaces of this important catalyst.

Qualitative models have also been discussed above for the marcasite (FeS_2) - arsenopyrite (FeAsS) – loellingite ($FeAs_2$) series of minerals, including ligand field and MO/band model approaches. Tossell et al. (1981) and Tossell (1984) have suggested that these models give

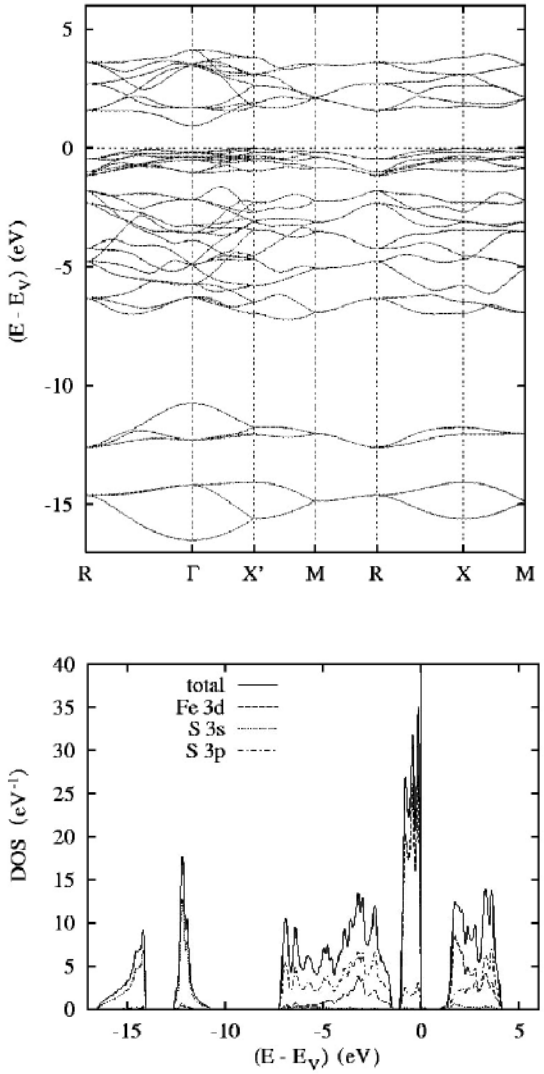

Figure 14. The calculated electronic structure of pyrite: (a) band structure of FeS_2 along selected symmetry lines within the first Brillouin zone of the simple cubic lattice; (b) total and partial densities of states. [Used with permission from Eyert et al. (1998), *Phys. Rev. B*, Vol. 57, Figs. 4 and 5, p. 6353. © 1998 American Physical Society.]

inadequate attention to the influence of the dianion electron distribution on the structures adopted in these compounds; they used MO calculations on the dianion units along with qualitative MO arguments to provide another interpretation. Here, attention is focused on the highest occupied MO of the electron donor and lowest unoccupied MO of the electron acceptor and their energies and overlaps. For example, the calculated MO scheme for S_2^{2-} has 14 electrons filling orbitals up to a $1\pi_g^*$ antibonding orbital (see Fig. 15) which can mix with metal *d* orbitals of σ symmetry to generate two pairs of orbitals, one oriented in the *xz* plane and the other in the *yz* plane (where *z* is the internuclear axis direction). Each pair consists of a metal-sulfur bonding orbital (π_b) stabilized relative to $1\pi_g^*$ and a destabilized antibonding orbital (π^*). In FeS_2, all of the π_b orbitals would be filled and all π^* empty. In $FeAs_2$, spectroscopic evidence suggests the iron may still be divalent and the dianion therefore As_2^{2-}, which would mean only 12 valence electrons, so that only one component of the π_b orbital set would be filled leading to the more distorted metal-anion coordination which is observed (see Fig. 15). Such arguments can be extended to other related dichalcogenides (listed in Table 1); for example, in FeAsS, the As end of the AsS group is effectively a "12 electron system" resulting in alternately greater or less distortion of the coordination of metals around the anion.

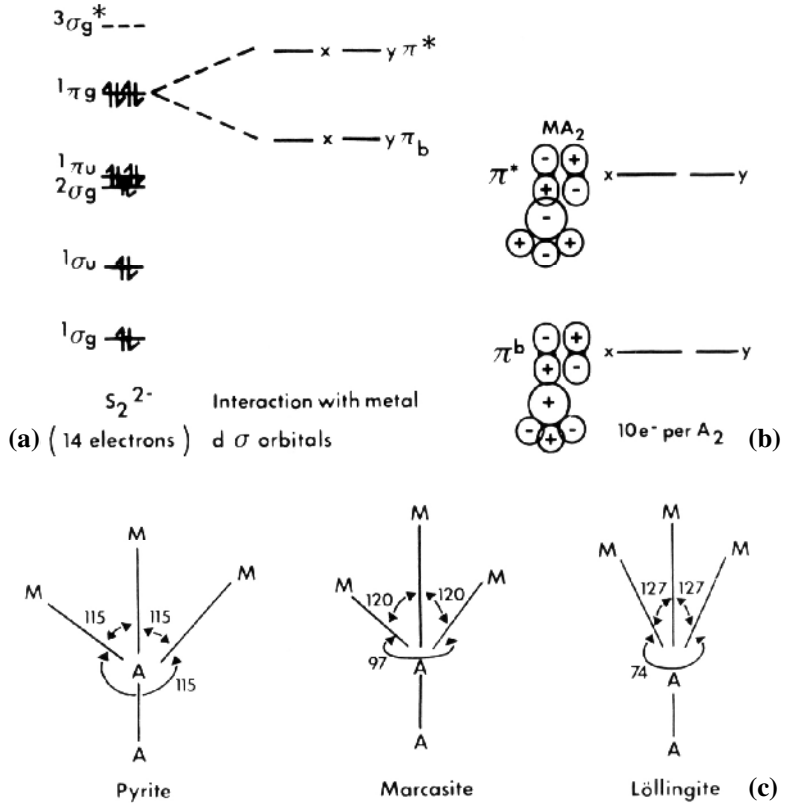

Figure 15. Models for the bonding in disulfides (after Tossell et al. 1981; Tossell and Vaughan 1992): (a) molecular orbital energy level diagram for the S_2^{2-} dianion and splitting of the highest energy orbital containing electrons on interaction with *M d*σ orbitals; (b) perturbed molecular orbitals formed by mixing of A_2 π_g* and *M d*σ; (c) geometries of *M* atoms about A in pyrite, marcasite, and loellingite structures. [Figures used by permission of Springer Verlag and Oxford Univeristy Press.]

Other (including complex) sulfides (pentlandites and metal-rich sulfides, thiospinels, layer structure sulfides, tetrahedrites)

The chemical bonding in a number of other sulfide minerals and mineral groups has been analyzed using both qualitative and quantitative models. Generally these minerals have been studied both because of their mineralogical importance, and because they present interesting challenges for theorists.

***Pentlandites* ($(Ni,Fe)_9S_8$ *and* Co_9S_8).** The minerals pentlandite and cobalt pentlandite form a solid solution series and are interesting examples of metal-rich sulfides. In pentlandite, a cube cluster of tetrahedrally coordinated cations has very short metal-metal distances (e.g., Co-Co = 2.505 Å); 32 of the 36 metal atoms in the unit cell occupy the tetrahedral sites of the cube clusters, with the other four in octahedral sites between the clusters (see Makovicky 2006, this volume). Tossell and Vaughan (1992) reviewed qualitative MO/band models for Co_9S_8 and discussed the reported metallic conductivity and Pauli paramagnetism used to make inferences about electronic structure.

Burdett and Miller (1987) pointed out the inadequacies of a ligand field analysis of the pentlandites, going on to analyze the cube clusters using MO calculations. Chauke et al. (2002) performed *ab initio* calculations using DFT. They were able to rationalize the high stability of the Co_9S_8 (and $Fe_5Ni_4S_8$) stoichiometries in terms of their Fermi levels falling in a pseudo(band)gap corresponding to an average number of electrons per atom of 7.58. They also performed calculations on Co_8S_8 which demonstrated the importance of the additional (octahedral) metal atoms to the stability of the structure, and calculated equilibrium lattice parameters and heats of formation in good agreement with experiment (the former being 1% smaller than experiment, the latter being calculated as –91.5 kJ/mole versus an experimental value of –85.1 kJ/mole). Raybaud et al. (1997b) in their *ab initio* DFT calculations on Co_9S_8 also found that the Fermi level falls at a deep pseudogap between the lower part of the Co 3*d* band (which has only weak interaction with the S 3*p* band) and the upper part which shows appreciable hybridization with the S 3*p*σ* states.

***Other metal-rich sulfides* (Ni_3S_2, Cu_2S, Ag_2S).** A number of sulfides in addition to pentlandite form phases with a metal:sulfur ratio > 1. Heazlewoodite, Ni_3S_2, is a metallic conductor which exhibits Pauli paramagnetism, the properties of which have been studied in detail by Metcalf et al.(1994). As noted above, Gibbs et al. (2005) computed electron density distributions in Ni_3S_2 and analyzed them for bonded interactions, showing that Ni-Ni bond paths form contiguous, highly branched networks in this "Ni 3*d* metallic conductor". Raybaud et al. (1997) also studied this phase and report calculated (total, local and partial) densities of states. Their electronic structure shows an overall similarity to that of the millerite and NiAs-structure forms of NiS, with the Fermi level separating the Ni orbitals interacting with the S 3*p*σ*, π band complex from the Ni 3*d* band.

The binary copper sulfides are more complex structurally than their formulae suggest (see Makovicky 2006, this volume); in chalcocite (Cu_2S) copper occurs in two kinds of triangular coordination. Experimental investigations of the electronic structure of Cu_2S include studies of valence region X-ray emission and photoelectron spectra (Domashevskaya et al. 1976; Nakai et al. 1978; Folmer and Jellinek 1980) and of S K and SL edge XANES (Li et al. 1994). These experimental data have been interpreted using MO cluster calculations (Tossell and Vaughan 1981) which suggest that the top of the valence band is comprised of Cu 3*d* states, with the S 3*p* non-bonding levels being significantly more tightly bound.

The binary silver sulfide Ag_2S (acanthite) is also structurally complex (see Makovicky 2006, this volume); half of the silver atoms occur in a twofold, nearly linear, coordination and half in a distorted tetrahedral coordination. X-ray emission and XPS data are available for Ag_2S (e.g., Domashevskaya et al. 1976) and MO calculations have been performed for

the AgS_2^{3-} and AgS_4^{7-} clusters (Tossell and Vaughan 1981). The calculations suggest that, in contrast to Cu_2S, the top of the valence band is comprised of S 3*p* non-bonding orbitals with, below them, the main Ag-S bonding orbitals, and the Ag 3*d* orbitals "buried"~ 4 eV beneath the top of the valence band. For further discussion of acanthite, chalcocite and related phases see Tossell and Vaughan (1981, 1992).

Thiospinels. The thiospinels, a group of sulfide minerals and synthetic compounds with the spinel structure have, therefore, both tetrahedrally and octahedrally coordinated metals in phases of the type $A^{tet}(B_2^{oct})S_4$ and with the possibilities of "formally" divalent and trivalent cations in both A and B sites. However, many of the thiospinels exhibit metallic behavior with valence electrons delocalized between tetrahedral and octahedral cations, so that formal valencies are not applicable. These materials have been well characterized as regards their electrical and magnetic properties but spectroscopic data are limited. In early qualitative work on bonding, Goodenough (1969) and Vaughan et al. (1971) were able to rationalize those properties and the solid solution limits found in the thiospinels using MO/band models. Such models were developed further by Vaughan and Tossell (1981) using MO calculations on appropriate clusters. The magnetic and Mössbauer parameters of greigite (Fe_3S_4) have also been discussed on the basis of similar (MS-SCF-X_α) MO calculations by Braga et al. (1988). A more detailed account of work on bonding in thiospinels is given in Tossell and Vaughan (1992).

Layer structure sulfides (MoS$_2$, CuS, FeS). Molybdenite (MoS_2), a diamagnetic, moderate band gap semiconductor, has been much studied by physicists because of its interesting properties and, as seen elsewhere in this volume, has been subjected to a wide range of spectroscopic techniques, both as a bulk material and with respect to its surface chemistry (see Wincott and Vaughan 2006; Rosso and Vaughan 2006b; this volume). A simple band model for MoS_2 has already been presented and discussed in the context of understanding the optical absorption spectrum (Wincott and Vaughan 2006). Many band structure calculations have been performed on MoS_2 and the earlier work has been reviewed by Calais (1977); later studies have involved both cluster (de Groot and Haas 1975; Harris 1982) and band structure (Coehoorn et al. 1987) calculations, some of which have also already been presented in the context of interpreting spectroscopic data. Molybdenite was one of the large number of sulfides studied using DFT calculations by Raybaud et al. (1997) who also provide a good summary of previous experimental and computational work. Their results confirm the importance of the ligand field splitting (in trigonal-prismatic coordination) of the transition metal *d* states, resulting from covalent Mo *d* – S *p* bonding interactions. The bulk, as well as the surface electronic structure of MoS_2 is discussed in some detail elsewhere in this volume, and the data of Raybaud et al. (1997) for the DOS of bulk MoS_2 are illustrated (Rosso and Vaughan 2006b; see their Fig. 38).

Covellite (CuS) has a more complex structure than its formula suggests, with Cu in both tetrahedral and triangular coordination and disulfide units in the structure. It is also a metallic conductor (see Pearce et al. 2006, this volume). Investigations of the electronic structure of covellite have been performed experimentally using K-edge and L-edge XANES (Li et al, 1994b), S K_β and S $L_{2,3}$ X-ray emission spectroscopy (Sugiura et al. 1974, Kurmaev et al. 1998), and X-ray photoelectron spectroscopy (Nakai et al. 1978; Folmer et al. 1980; Kurmaev et al. 1998). The spectroscopic data on CuS are discussed elsewhere in this volume (Wincott and Vaughan 2006). These spectra have been interpreted using MO calculations on appropriate cluster units, with the calculations then used to propose a simple band model for covellite (Vaughan and Tossell 1980, 1981); see Figure 16. Although calculations were initially performed on CuS_3^{4-} and CuS_4^{7-}, the metallic conductivity and spectroscopic evidence for essentially monovalent copper being present, led to the suggestion that charge should flow from the $4t_2$ orbital on the tetrahedral "Cu^{+}" to the 4*e* orbital on the triangular "Cu^{2+}". This was modeled by performing a cluster calculation on $CuS_4^{6.5-}$ and using this with the CuS_3^{5-} calculation to give the composite "one-electron" band model shown in Figure 16. More recent calculations using extended Hückel tight binding

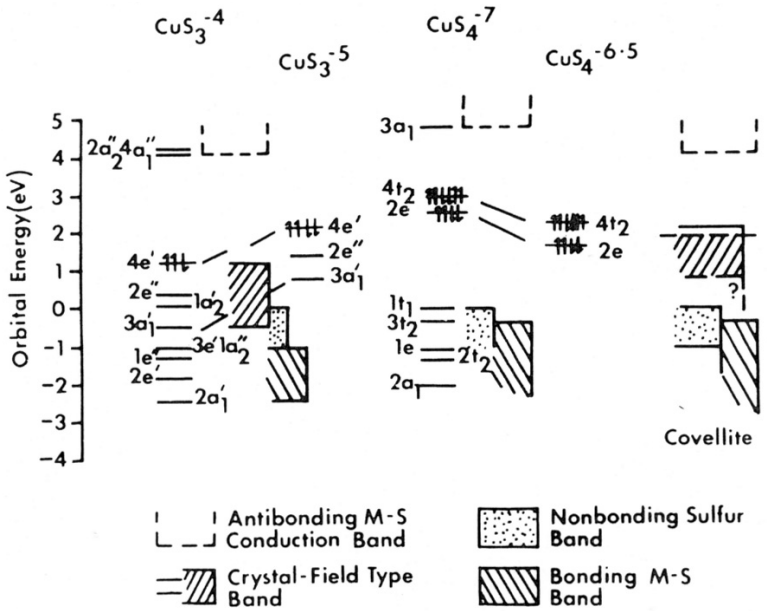

Figure 16. An electronic structure model for covellite (CuS) based on calculations using an MO cluster method (multiple scattering X_α). Discrete energy levels are shown for the clusters CuS_3^{4-}, CuS_3^{5-}, CuS_4^{7-}, $CuS_4^{6.5-}$ and a composite "one electron" band model energy level diagram for the mineral. (After Vaughan and Tossell 1980.)

methods (Liang and Whangbo 1993) and HF calculations on the periodic covellite structure (Rosso and Hochella 1999) largely confirm this model. One point of apparent difference is that these latter studies suggest that the top of the valence band is comprised predominantly of S 3*p* states, in contrast to the crystal field-like Cu 3*d* states suggested by the MO calculations. Formal charges in CuS appear to be best described by the formula $(Cu^+)_3(S^{2-})(S^{2-})$, where Cu in both tetrahedral and trigonal planar sites is approximately monovalent, the S^{2-} sites are the trigonal planar ligands, and the S_2^- sites are three of the four tetrahedral ligand sites (Nakai et al. 1978; Liang and Whangbo 1993; Rosso and Hochella 1999).

Mackinawite (FeS), the layer structured tetragonal iron monosulfide, is of great environmental importance because it is the first sulfide formed in many low *T* aqueous environments (see elsewhere in this volume; e.g., Rickard and Luther 2006). Data on many of the properties of this phase are lacking, as it occurs only as fine particles. However, Welz and Rosenberg (1987) performed band structure calculations on this form of FeS using a DFT (LMTO) method suggesting it to be metallic with conduction bands of mainly *d*-electron character. The calculations suggest that direct Fe-Fe interactions across the edge-sharing FeS_4 tetrahedra in the structure are responsible for a reduced density of states at the Fermi level and absence of magnetic ordering, even at very low temperature (see Wincott and Vaughan 2006; this volume).

Tetrahedrites. The minerals forming the complete solid solution series from tetrahedrite ($Cu_{12}Sb_4S_{13}$) to tennantite ($Cu_{12}As_4S_{13}$) are economically and environmentally important because of the numerous substitutions that can occur for Cu in the structure (this includes Zn, Fe, Cd, Hg, Ag). The crystal chemistry of this mineral family is complex. The structure of $Cu_{12}Sb_4S_{13}$ has half of the Cu atoms in tetrahedral and half in trigonal sites, Sb bonded to three S atoms with a "lone pair" of electrons extending in a fourth tetrahedral direction, and twelve of the S atoms in tetrahedral and the thirteenth S atom in octahedral coordination (see Makovicky,

2006, this volume). Considering just this three component endmember, there is also a variation in stoichiometry which accommodates Cu-rich phases with compositions bounded by the line $Cu_{14}Sb_4S_{13} - Cu_{12}Sb_{4.67}S_{13}$ in the Cu-Sb-S system (Johnson and Jeanloz 1983). The substitutions in this mineral group have been extensively investigated using X-ray diffraction, and X-ray absorption and ^{57}Fe Mössbauer spectroscopies (see Wincott and Vaughan 2006, this volume). Despite the complexity of these materials, there have been qualitative and quantitative models presented to describe the electronic structure of compositions within the Cu-Sb-S system. Johnson and Jeanloz (1983) used concepts developed for the description of alloys to predict correctly compositional limits and electrical properties. In this work, the arguments center on phases being stable at a particular electron-to-atom ratio due to the filling of Brillouin zones with electrons. Bullett and Dawson (1986) and Bullett (1987) used non-empirical atomic orbital based techniques to calculate the band structure of Cu-Sb-S system tetrahedrites (see Fig. 17), showing that $Cu_{12}Sb_4S_{13}$ is intrinsically electron deficient. Calculations on the composition $Cu_{14}Sb_4S_{13}$ showed a filled valence band with an energy gap of 0.9 eV between highest filled and lowest empty states. It is suggested that in this "copper rich" variant, the two additional Cu atoms per formula unit are accommodated by displacing two tetrahedrally coordinated Cu atoms into a third kind of interstitial site. The calculated density of states for the different kinds of Cu atoms and displaced coppers are shown in Figure 17.

CONCLUDING REMARKS

Recent decades have seen remarkable advances in our attempts to calculate the electronic structures of minerals and related materials. It is now possible to use *ab initio* quantum mechanical calculations to predict structures and properties that, in many cases, show excellent agreement with experiment, and such calculations will surely be at the forefront of future work.

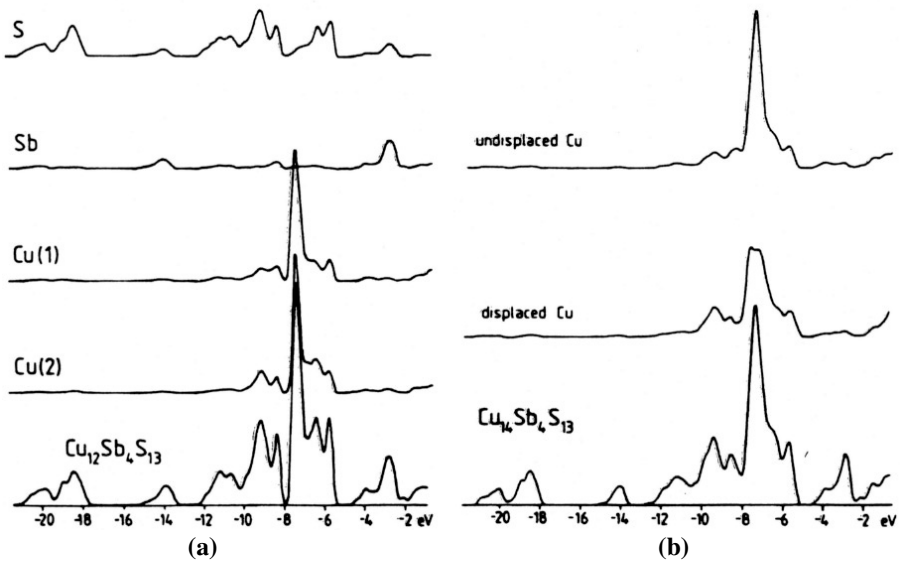

Figure 17. The calculated densities of states in the two tetrahedrites $Cu_{12}Sb_4S_{13}$ and $Cu_{14}Sb_4S_{13}$ and its local site projections for S, Sb, and various types of Cu atom. In the copper-rich phase the copper contribution for undisplaced and displaced (interstitial) Cu sites are compared. [Used with permission of Springer-Verlag from Bullet (1987), *Phys. Chem. Min.,* Vol. 14, Fig. 1, p. 486.]

There have been parallel advances in experimental methods, particularly those spectroscopic methods that can provide direct information on electronic structure, such as photoemission and X-ray absorption spectroscopies (see Wincott and Vaughan 2006, this volume). As the discussions presented in this chapter show, the sulfides are a diverse and complex group of materials in terms of their electronic structures. A range of both quantitative and qualitative approaches has proved valuable in our attempts to the understand structure and bonding in sulfides, and this is likely to continue. Qualitative models will continue to be of value in providing conceptual advances in understanding. However, these will be guided by new concepts, or by methods of analysis that provide much more rigorous definitions of older concepts such as "charge" or "covalency" used to describe sulfide minerals. Quantitative calculations using *ab initio* methods are being consistently incrementally improved, but larger leaps forward in this regard are already on the horizon. In the future, vastly improved accuracy is likely to come in the form of multiconfiguration or excited state electronic structure calculations.

ACKNOWLEDGMENTS

DJV acknowledges the contributions of the Natural Environment Research Council and the Engineering and Physical Sciences Research Council in supporting his research in the mineral sciences. DJV also wishes to thank Jack Tossell and Michele Warren for valuable discussions regarding sulfide electronic structure studies. Helen Weedon and Richard Hartley are thanked for help in the preparation of the manuscript. KMR acknowledges the support of the U.S. Department of Energy (DOE), Office of Basic Energy Sciences, Geosciences Division, and the Stanford Environmental Molecular Sciences Institute (EMSI) jointly funded by the National Science Foundation and the DOE Office of Biological and Environmental Research (OBER). The W. R. Wiley Environmental Molecular Science Laboratory (EMSL) at Pacific Northwest National Laboratory (PNNL) is a national scientific user facility sponsored by the OBER. PNNL is operated for the DOE by Battelle Memorial Institute under contract DE-AC06-76RLO 1830.

REFERENCES

Apra E, Bylaska EJ, de Jong W, Hackler MT, Hirata S, Pollack L, Smith DMA, Straatsma TP, Windus TL, Harrison RJ, Nieplocha J, Tipparaju V, Kumar M, Brown E, Cisneros G, Dupuis M, Fann GI, Fruchtl H, Garza J, Hirao K, Kendall R, Nichols JA, Tsemekhman K, Valiev M, Wolinski K, Anchell J, Bernholdt D, Borowski P, Clark T, Clerc D, Dachsel H, Deegan M, Dyall K, Elwood D, Glendening E, Gutowski M, Hess A, Jaffe J, Johnson B, Ju J, Kobayashi H, Kutteh R, Lin Z, Littlefield R, Long X, Meng B, Nakajima T, Niu S, Rosing M, Sandrone G, Stave M, Taylor H, Thomas G, van Lenthe J, Wong A, Zhang Z (2003) NWChem: A computational chemistry package designed to run on high-performance parallel supercomputers, version 4.5. Pacific Northwest National Laboratory

Bader RFW (1990) Atoms in Molecules. Oxford Science Publications

Bader RFW (1998) A bond path: a universal indicator of bonded interactions. J Phys Chem A 102:7314-7323

Bauschlicher CW Jr., Maitre P (1995) Theoretical study of the first transition row oxides and sulfides. Theorchim Acta 90:189-203

Becke AD (1993) A new mixing of Hartree-Fock and local density functional theories. J Chem Phys 98:1372-1377

Becke AD (1998) A new inhomogeneity parameter in density-functional theory. J Chem Phys 109:2092-2098

Becker U, Rosso KM (2001) Step edges on galena (100): Probing the basis for defect driven surface reactivity at the atomic scale. Am Mineral 86:862-870

Bernard JE, Zunger A (1987) Electronic structure of ZnS, ZnSe, ZnTe and their pseudobinary alloys. Phys Rev B 36:3199-3228

Bither TA, Bouchard RJ, Cloud WH, Donohue PC, Siemons WJ (1968) Transition metal pyrite dichalcogenides. High pressure synthesis and correlation of properties. Inorg Chem 7:2208-2220

Bocquet AE, Mamiya K, Mizokawa T, Fujimori A, Miyadai T, Takahashi H, Mori M, Suga S (1996) Electronic structure of 3d transition metal pyrites MS_2 (M = Fe, Co or Ni) by analysis of the M 2p core-level photoemission spectra. J Phys Condens Matt 8:2389-2400

Braga M, Lie SK, Taft CA, Lester WA Jr. (1988) Electronic structure, hyperfine interaction, and magnetic properties for iron octahedral sulfides. Phys Rev B 38:10837-10851

Bullett DW (1982) Electronic structure of 3d pyrite- and marcasite-type sulfides. J Phys C 15:6163-6174

Bullet DW (1987) Applications of atomic-orbital methods to the structure and properties of complex transition-metal compounds. Phys Chem Mineral 14: 485-491

Bullet DW, Dawson WG (1986) Bonding relationships in some ternary and quaternary phosphide and tetrahedrite structures ($Ag_6M_4P_{12})M_6$', $Cu_{12+x}Sb_4S_{13}$, $Cu_{14-x}Sb_4S_{13}$, $Ln_6Ni_6P_{17}$. J Phys C 19:5837-5847

Burdett JK, Miller GJ (1987) Polyhedral clusters in solids: the electronic structure of pentlandite. J Am Chem Soc 109:4081-4091

Burns RG (1993) Mineralogical Applications of Crystal Field Theory. (2nd edition) Cambridge Univ. Press

Burns RG, Vaughan DJ (1970) Interpretation of the reflectivity behavior of ore minerals. Am Mineral 55:1576-1586

Car R, Parrinello M (1985) Unified approach for molecular dynamics and density functional theory. Phys Rev Lett 55:2471-2244

Calais JL (1977) Band structure of transition metal compounds. Adv Phys 26:847-885

Catlow CRA (1997) Need and scope of modelling techniques. *In* Computer Modelling in Inorganic Crystallography. Catlow CRA (ed). Academic Press, p. 1-22

Cardona M, Greenaway DL (1964) Optical properties and band structure of group IV-VI and group V materials. Phys Rev 133:1685-1697

Charnock JM, Henderson CMB, Mosselmans JFW, Pattrick RAD (1996) 3d transition metal L-edge X-ray absorption studies of the dichalcogenides of Fe, Co and Ni. Phys Chem Mineral 23:403-408

Chauke HR, Nguyen-Manh D, Ngoepe PE, Pettifor DG, Fries SG (2002) Electronic structure and stability of the pentlandites Co_9S_8 and $(Fe,Ni)_9S_8$. Phys Rev B 66:155105

Coehoorn R, Haas C, Dijkstra J, Flipse CJF, De Groot RA, Wold A (1987) Electronic structure of molybdenum diselenide, molybdenum disulfide and tungsten diselenide. I. Band-structure calculations and photoelectron spectroscopy. Phys Rev B 35:195-202

Cygan RT, Kubicki JD (eds) (2001) Molecular Modeling Theory: Applications in the Geosciences. Reviews in Mineralogy and Geochemistry. Vol. 42. Mineralogical Society of America

de Groot RA, Hass C (1975) Multiple Scattering theory-Xα .Calculations on molybdenum disulfide and some related compounds. Solid State Comm 17:887-890

Domashevskaya EP, Terekhov, V.A, Marshakova LN, Ugai Ya A, Nefedov VI, Sergushin NP (1976) Participation of d-electrons of metals of groups I, II, and III in chemical bonding with sulfur. J Elec Spec Rel Phen 9: 261-267

Edelbro R, Sandstrom A, Paul J (2003) Full potential calculations on the electron bandstructures of sphalerite, pyrite and chalcopyrite. Appl Surf Sci 206: 300-313

Eyert V, Hock K-H, Fiechter S, Tributsch H (1998) Electronic structure of FeS_2: The crucial role of electron-lattice interaction. Phys Rev B 57:6350-6359

Farberovich, OV, Kurganskii S I Domashevskaya EP (1980) Problems of the OPW method. II. Calculation of the band structure of zinc sulfide and cadmium sulfide. Phys Status Solidi B 97:631-640

Ferrer IJ, Nevskaia DM, de las Herras C, Sanchez C (1990) About the band gap nature of FeS_2 as determined from optical and photoelectrochemical measurements. Sol State Comm 74:913-916

Fleet ME (2006) Phase equilibria at high temperatures. Rev Mineral Geochem 61:365-419

Folkerts W, Sawatzky GA, Haas C, de Groot RA, Hillebrecht FU (1987) Electronic structure of some 3d transition-metal pyrites. J Phys C 20:4135-4144

Folmer JCW, Jellinek F (1980) The valence of copper in sulfides and selenides: An X-ray photoelectron spectroscopy study. J Less Comm Met 76:153-162

Folmer JCW, Jellinek F, Calis GHM (1988) The electronic structure of pyrites, particularly copper disulfide and iron copper selenide ($Fe_{1-x}Cu_xSe_2$): An XPS and Mössbauer study. J Sol Stat Chem 72:137-144

Fujimori A, Mamiya K, Mizokawa T, Miyadai T,.; Sekiguchi T, Takahashi H, Mori N, Suga S (1996) Resonant photoemission study of pyrite-type NiS_2, CoS_2 and FeS_2. Phys Rev B 54:16329-16332

Fujisawa M, Suga S, Mizokawa T, Fujimori A, Sato K (1994) Electronic structures of $CuFeS_2$ and $CuAl_{0.9}Fe_{0.1}S_2$ studied by electron and optical spectroscopies. Phys Rev B 49:7155-7164

Gale JD (2001) Simulating the crystal structures and properties of ionic materials from interatomic potentials. Rev Mineral Geochem 42:37-62

Gamblin SD, Urch DS (2001) Metal Kβ X-ray emission spectra of first row transition metal compounds. J Elect Spect Rel Phenom 113:179-192

Gerson AR, Bredow T (2000) Interpretation of sulfur 2p XPS spectra in sulfide minerals by means of ab initio calculations. Surf Int Anal 29:145-150

Gibbs GV, Tamada O, Boisen MB Jr, Hill FC (1999) Laplacian and bond critical point properties of the electron density distributions of sulfide bonds: A comparison with oxide bonds. Am Mineral 84:435-446

Gibbs GV, Downs RT, Prewitt CT, Rosso KM, Ross NL, Cox DF (2005) Electron density distributions calculated for the nickel sulfides millerite, vaesite, and heazlewoodite and nickel metal: A case for the importance of Ni-Ni bond paths for electron transport. J Phys Chem B 109:21788-21795

Goodenough JB (1967) Description of transition metal compounds. Application to several sulfides. Coll Int Centre Nat Recherche Sci 157:263-90, discussion 290-292

Goodenough JB (1969) Descriptions of outer d-electrons in thiospinels. J Phys Chem Solids 30:261-280

Goodenough JB (1972) Energy bands in TX_2 compounds with pyrite, marcasite and arsenopyrite structures. J Solid State Chem 5:144-152

Goodenough JB (1997) Localized-itinerant electronic transitions in oxides and sulfides. J Alloys Comp 262: 1-9

Gopalakrishnan J, Murugesan T, Hegde MS, Rao CNR (1979) Study of transition metal monosulfides by photoelectron spectroscopy. J Phys C 12:5255-5261

Grandke T, Ley L, Cardona M (1978) Angle resolved UV photoemission and electronic band structures of the lead chalcogenides. Phys Rev B 18:3847-3871

Gurin VS (1998) Observation and simulation of PbS nanocrystal formation at the initial steps. Macromolecular Symposia 136, 2nd International Conference on Chemistry of Highly-Organized Substances and Scientific Principles of Nanotechnology, 13-16

Hamad S, Cristol S, Catlow CRA (2002) Surface structures and crystal morphology of ZnS: A computational study. J Phys Chem 106:11002-11008

Hamajima T, Kambara T, Gondaira KI, Oguchi T(1981) Self-consistent electronic structures of magnetic semiconductors by a discrete variational X_α calculation III. Chalcopyrite $CuFeS_2$. Phys Rev B 24:3349-3353

Harris S (1982) Study of the electronic structure of first and second row transition metal sulfides using SCF-SW-Xα cluster calculations. Chem Phys 67:229-237

Hemstreet LA Jr. (1975) Cluster calculations of the effect of single vacancies of the electronic properties of lead(II) sulfide. Phys Rev B 11:2260-2270

Hobbs D, Hafner J (1999) Magnetism and magneto-structural effects in transition-metal sulfides. J Phys Cond Matt 11:8197-8222

Huang YS, Huang JK, Tsay MY (1993) An electroreflectance study of FeS_2. J Phys Cond Matt 5: 7827-7836

Hulliger F (1968) Crystal chemistry of the chalcogenides and pnictides of the transition elements. Struct Bond 4:83-229

Ikoma H, Matoba M, Mikami M, Anzai S (1995) Effect of 4d transition metal atom Rh doping on thermoelectric power, magnetic susceptibility, thermal expansion and X-ray photoemission spectra in the charge transfer type non-metallic state of NiS. J Phys Soc Japan 64:2600-2608

Johnson ML, Jeanloz R (1983) A Brillouin-zone model for compositional variation in tetrahedrite. Am Mineral 68:220-226

Kjekshus A, Nicholson DG (1971) The significance of π back bonding in compounds with the pyrite, marcasite and arsenopyrite type structures. Acta Chem Scand 25:866-876

Krishnakumar SR, Shanthi N, Sarma DD (2002) Electronic structure of millerite NiS. Phys Rev B 66:115105

Kurmaev EZ, van Ek J, Ederer DL, Zhou L, Callcott TA, Perera RCC, Chernashenko VM, Shamin SN, Tromifova VA, Bartkowski S, Neumann M, Fujimori A, Moloshag VP (1998) Experimental and theoretical investigation of the electronic structure of transiotion metal sulphides: CuS, FeS_2 and $FeCuS_2$. J Phys Cond Matt 10:1687-1697

Lavrentyev AA, Gabrelian BV, Nikiforov IYa, Rehr JJ, Ankudinov AL (2004) The electron energy structure of some sulfides of iron and copper. J Elec Spec Rel Phenom 137-140:495-498

Lawniczak-Jablonska K, Iwanowski RJ, Golacki Z, Traverse A, Pizzini S, Fontaine A, Winter I, Hormes J (1996) Local electronic structure of ZnS and ZnSe doped by Mn, Fe, Co, and Ni from X-ray absorption near-edge structure studies. Phys Rev 53:1119-1128

Laihia R, Leiro, JA, Kokko K, Mansikka K (1996) The X-ray $K\beta_{2.5}$ emission band and the electronic structure of Zn, ZnS and Znse crystals. J Phys Cond Matt 8:6791-6801

Laihia R, Kokko K, Hergert W, Leiro JA (1998) K-emission spectra of Zn, ZnS, and ZnSe within dipole and quadrupole approximations. Phys Rev B 58:1272-1278

Lee CT, Yang WT, Parr RG (1988) Development of the Colle-Salvetti correlation energy formula into a functional of the electron density. Phys Rev B 37:785-789

Leiro JA, Laajalehto K, Kartio I, Heinonen MH (1998) Surface core-level shift and phonon broadening in PbS (100). Surf Sci 412/413, L918-L923

Ley L, Pollak RA, McFeely FR, Kowalczyk SP, Shirley DA (1974) Total valence-band densities of states of [Groups] III-V and II-VI compounds from X-ray photoemission spectroscopy. Phys Rev B 9:600-621

Li EK, Johnson KH, Eastman DE, Freeouf JL (1974) Localized and bandlike valence-electron states in iron sulfide (FeS_2) and nickel sulfide (NiS_2). Phys Rev Lett 32:470-472

Li, D, Bancroft GM, Kasrai M, Fleet ME, Feng XH, Tan KH, Yang BX (1994a) Sulfur K- and L-edge XANES and electronic structure of zinc, cadmium and mercury monosulfides: a comparative study. J Phys Chem Solids 55:535-543

Li D, Bancroft GM, Kasrai M, Fleet ME, Feng XH, Yang BX, Tan KH (1994b) S K-edge and L-edge XANES and electronic structure of some copper sulfide minerals. Phys Chem Mineral 21:317-324

Li D, Bancroft GM, Kasrai M, Fleet ME, Yang BX, Feng XH, Tan K, Peng M (1994c) Sulfur K- and L-edge X-ray absorption spectroscopy of sphalerite, chalcopyrite and stannite. Phys Chem Mineral 20:489-499

Liang W, Whangbo MH (1993) Conductivity anisotropy and structural phase transition in covellite CuS. Solid State Comm 85:405-408

Lutz HD, Zminscher J (1996) Lattice dynamics of pyrite FeS_2 polarizable-ion model. Phys Chem Mineral 23: 497-502

Ma J-X, Jia Y, Song Y-L, Liang E-J, Wu L-K, Wang F, Wang X-C, Hu X (2004) The geometric and electronic properties of the PbS, PbSe and PbTe (001) surfaces. Surf Sci 551:91-98

Makovicky E (2006) Crystal structures of sulfides and other chalcogenides. Rev Mineral Geochem 61:7-125

Martins JL, Troullier N, Wei SH (1991) Pseudopotential planewave calculations for zinc sulfide. Phys Rev B 43:2213-2217

Marusak LA, Tongson LL (1979) Soft X-ray emission and Auger electron spectroscopic study of iron(II) sulfide, iron sulfides $Fe_{0.9}S$, $Fe_{0.875}S$, and $Fe_{0.5}S$. J Appl Phys 50:4350-4355

Matsukawa T, Obashi M, Nakai S, Sugiura C (1978) The K absorption spectra of FeS_2, CoS_2 and NiS_2. Jap J Appl Phys 17 (Suppl 17-2) 184-186

McFeely FR, Kowalczyk S, Ley L, Pollak RA, Shirley DA (1973) High-resolution X-ray photoemission spectra of lead sulfide, lead selenide, and lead telluride valence bands. Phys Rev B 7:5228-2237

Merkel S, Jephcoat AP, Shu J, Mao H-K, Gillet P, Hemley RJ (2002) Equation of state, elasticity and shear strength of pyrite under high pressure. Phys Chem Mineral 29:1-9

Mian M, Harrison NM, Saunders VR, Flavell WR (1996) An ab initio Hartree-Fock investigation of galena (PbS). Chem Phys Lett 257:627-632

Mikhlin Y, Tomashevich Y, Pashkov GL, Okotrub AV, Asanov IP, Mazalov LN (1998) Electronic structure of the non-equilibrium iron-deficient layer of hexagonal pyrrhotite. Appl Surf Sci 125:73-84

Mikhlin Y, Tomashevich Y, Tauson V, Vyalikh D, Molodtsov S, Szargan R (2005) A comparative X-ray absorption near-edge structure study of bornite Cu_5FeS_4, and chalcopyrite, $CuFeS_2$. J Elec Spec Rel Phenom 142:83-88

Mosselmans JFW, Pattick RAD, van der Laan G, Charnock JM, Vaughan DJ, Henderson CMB, Garner CD (1995) X-ray absorption near-edge spectra of transition metal disulfides FeS_2 (pyrite and marcasite), CoS_2, NiS_2 and CuS_2, and their isomorphs FeAsS and CoAsS. Phys Chem Mineral 22:311-317

Muscat J, Klauber C (2001) A combined ab initio and photoelectron study of galena (PbS). Surf Sci 491:226-238

Muscat J, Hung A, Russo S, Yarovsky I (2002) First-principles studies of the structural and electronic properties of pyrite FeS_2. Phys Rev B 65:054107

Nakai I, Sugitani Y, Nagashima K, Niwa Y (1978) X-ray photoelectron spectroscopic study of copper minerals. J Inorg Nucl Chem 40:789-791

Nickel EH (1968) Structural stability of minerals with the pyrite, marcasite, arsenopyrite and loellingite structures. Can Mineral 9:311-321

Nickel EH (1970) The application of ligand field concepts to an understanding of the structural stabilities and solid solution limits of sulfides and related minerals. Chem Geol 5:233-241

Ohsawa A Yamamoto H, Watanabe H (1974) X-ray photoelectron spectra of valence electrons in iron disulfide, cobalt disulfide, and nickel disulfide. J Phys Soc Jap 37:568

Ollonqvist T, Kaurila T, Isokallio M, Punkkinen M, Vayrynen J (1995) Inverse photoemission and photoemission spectra of the PbS (001) surface. J Elec Spec Rel Phenom 76:729-734

Pantelides S, Harrison WA (1975) Structure of the valence band of zincblende-type semiconductors. Phys Rev B 11:3006-3011

Pattrick RAD, Mosselmans JFW, Charnock JM (1998) An X-ray absorption study of doped sphalerites. Euro J Mineral 10:239-249

Pearce CI, Pattrick RAD, Vaughan DJ (2006) Electrical and Magnetic properties of sulfides. Rev Mineral Geochem 61:127-180

Pearson WD (1965) Compounds with the marcasite structure. Z Kristallogr 121:449-462

Perdew JP, Wang Y (1992) Accurate and simple analytic representation of the electron gas correlation energy. Phys Rev B 45:13244-13249

Perez-Dieste V, Crain JN, Kirakosian A, McChesney JL, Arenholz E, Young AT, Denlinger JD, Ederer DL, Callcott TA, Lopez-Rivera SA, Himpsel FJ (2004) Unoccupied orbitals of 3d transition metals in ZnS. Phys Rev B 70:085205

Prince KC, Matteucci M, Kuepper K, Chiuzbaian SG, Bartkowski S, Neumann M (2005) Core-level spectroscopic study of FeO and FeS_2. Phys Rev B 71:085102.

Rabii S, Lasseter RH (1974) Band structure of PbPo and trends in the Pb chalcogenides. Phys Rev Lett 33: 703-704

Raybaud P, Kresse G, Hafner J, Toulhoat H (1997) *Ab initio* density functional studies of transition metal sulfides; I. Crystal structure and cohesive properties. J Phys Cond Matt 9:11085-11106
Raybaud P, Hafner J, Kresse G, Toulhoat H (1997) *Ab initio* density functional studies of transition metal sulfides; II. Electronic structure. J Phys Cond Matt 9:11107-11140
Rickard D, Luther GW III (2006) Metal sulfide complexes and clusters. Rev Mineral Geochem 61:421-504
Rohrbach A, Hafner J, Kresse G (2003) Electronic correlation effects in transition-metal sulfides. J Phys Cond Matt 15:979-996
Rosso KM (2001) Structure and reactivity of semiconducting mineral surfaces: Convergence of molecular modeling and experiment. Rev Mineral Geochem 42:199-271
Rosso KM, Becker U, Hochella MF (1999) A UHV STM/STS and ab initio investigation of covellite (001) surfaces. Surf Sci 423:364-374
Rosso KM, Hochella MF (1999) Atomically resolved electronic structure of pyrite {100} surfaces: An experimental and theoretical investigation with implications for reactivity. Am Mineral 84:1535-1548
Rosso KM, Vaughan DJ (2006a) Reactivity of sulfide mineral surfaces. Rev Mineral Geochem 61:557-607
Rosso KM, Vaughan DJ (2006b) Sulfide mineral surfaces. Rev Mineral Geochem 61:505-556
Rueff J-P, Kao C-C, Struzhkin VV, Badro J, Shu J, Hemley RJ, Mao H K (1999) Pressure-induced high-spin to low-spin transition in FeS evidenced by X-ray emission spectroscopy. Phys Rev Lett 82:3284-3287
Saitoh T, Bocquet AE, Mizokawa T, Fujimori A (1995) Systematic variation of the electronic structure of 3d transition-metal compounds. Phys Rev 52:7934-7938
Sakkopoulos S, Vitoratos E, Argyreas T (1984) Energy-band diagram for pyrrhotite. J Phys Chem Solids 45: 923-928
Santoni A, Paolucci G, Santoro G, Prince KC, Christensen NE (1992) Band structure of lead sulphide. J Phys Cond Matt 4:6759-6768
Satta A, de Gironcoli S (2000) Surface structure and core-level shift in lead chalcogenide (001) surfaces. Phys Rev B 63:033302
Saunders VR, Dovesi R, Roetti C, Orlando R, Zicovich-Wilson CM, Harrison NM, Doll K, Civalleri B, Bush IJ, D'Arco P, Llunell M (2003) CRYSTAL03. University of Torino
Schoolar RB, Dixon JR (1965) Optical constants of lead sulfide in the fundamental absorption edge region. Phys Rev 137:667-670
Schroer P, Kruger P, Pollmann J (1993) First-principles calculation of the electronic structure of the wurtzite semiconductors ZnO and ZnS. Phys Rev 47:6971-6980
Schlegel A, Wachter P(1976) Optical properties, phonons, and electronic structure of iron pyrite (FeS_2). J Phys C 9: 3363-3369
Shannon RD (1981) Bond distances in sulfides and a preliminary table of sulphide crystal radii. *In:* Structure and Bonding in Crystals II. O'Keefe M, Navrotsky A (eds) Academic Press, p. 53-70
Sithole HM, Ngoepe PE, Wright K (2003) Atomistic simulation of the structure and elastic properties of pyrite (FeS_2) as a function of pressure. Phys Chem Mineral 30:615-619
Skinner WM, Nesbitt HW, Pratt AR (2004) XPS identification of bulk hole defects and itinerant Fe 3d electrons in natural troilite (FeS). Geochim et Cosmochim Acta 68:2259-2263
Soldatov AV, Kravtsova AN, Fleet ME, Harmer SL (2004) Electronic structure of MeS (Me = Ni, Co, Fe): X-ray absorption analysis. J Phys Cond Matt 16:7545-7556
Sowa H, Ahsbahs H, Schmitz W (2004) X-ray diffraction studies of millerite NiS under non-ambient conditions. Phys Chem Mineral 31:321-327
Stadele M, Moukara M, Majewski JA, Vogl P, Gorling A (1999) Exact exchange Kohn-Sham formalism applied to semiconductors. Phys Rev B 59:10031-10043
Stukel DJ, Euwema RN, Collins TC, Herman F, Kortum RL (1969) Self-consistent orthogonalised planewave and empirically refined orthogonalised planewave energy band models for cubic ZnS, ZnSe, CdS and CdSe. Phys Rev 179:740-751
Suga S, Inoue K, Taniguchi M, Shin S, Seki M, Sato K, Teranishi T (1983) Vacuum ultraviolet reflectance spectra and band structures of pyrites (FeS_2, CoS_2 and NiS_2) and NiO measured with synchrotron radiation. J Phys Soc Jap 52:1848-1856
Sugiura C (1994) Lα x-ray emission spectra and electronic structures of zinc and its compounds. J Phys Soc Jap 63:3763-3774
Sugiura C, Gohshi Y, Suzuki I (1974) Sulfur K_β X-ray emission spectra and electronic structures of some metal sulfides. Phys Rev B 10:338-343
Sugiura C, Suzuki I, Kashiwakura J Gohshi Y (1976) Sulfur K_β X-ray emission bands and valence-band structures of transition-metal disulfides. J Phys Soc Jap 40:1720-1724
Sugiura C, Yorikawa H, Muramatsu S (1997) Sulfur K_β X-ray emission spectra and valence-band structures of metal sulfides. J Phys Soc Jap 66:503-504
Svane A, Santi G, Szotek Z, Ternmerman WM, Strange P, Horne M, Vaitheeswaran G, Kandiana V, Petit L, Winter H (2004) Electronic structure of Sm and Eu chalcogenides. Phys Stat Sol B 241:3185-3192

Temmerman WM, Durham PJ, Vaughan DJ (1993) The electronic structures of the pyrite-type disulfides (MS_2, where M = manganese, iron, cobalt, nickel, copper, zinc) and the bulk properties of pyrite from local density approximation (LDA) band structure calculations. Phys Chem Mineral 20:248-54

Tossell JA (1977a) Theoretical studies of valence orbital binding energies in solid zinc sulfide, zinc oxide, and zinc fluoride. Inorg Chem 16:2944-2949

Tossell JA (1977b) SCF-X_α scattered wave MO studies of the electronic structure of ferrous iron in octahedral coordination with sulfur. J Chem Phys 66:5712-5719

Tossell JA (1984) A reinterpretation of the electronic structures of $FeAs_2$ and related minerals. Phys Chem Mineral 11:75-80

Tossell JA, Vaughan DJ (1981) Relationships between valence orbital binding energies and crystal structures in compounds of copper, silver, gold, zinc, cadmium, and mercury. Inorg Chem 20:3333-3340

Tossell JA, Vaughan DJ (1987) Electronic structure and the chemical reactivity of the surface of galena. Can Mineral 25:381-392

Tossell JA, Vaughan DJ (1992) Theoretical Geochemistry: Application of Quantum Mechanics in the Earth and Mineral Sciences. Oxford Univ Press

Tossell JA, Vaughan DJ, Burdett JK (1981) Pyrite, marcasite and arsenopyrite type minerals: Crystal chemical and structural principles. Phys Chem Mineral 7:177-184

Tossell JA, Urch DS, Vaughan DJ, Wiech G (1982) The electronic structure of $CuFeS_2$, chalcopyrite, from x-ray emission and x-ray photoelectron spectroscopy and X_α calculations. J Chem Phys 77:7-82

Tung YW, Cohen ML (1969) Relativistic band structure and electronic properties of tin telluride, germanium telluride, and lead telluride. Phy Rev 180:823-826

van der Heide H, Hemmel R, Van Bruggen CF, Haas C (1980) X-ray photoelectron spectra of 3d transition metal pyrites. J Solid State Chem 33:17-25

Vaughan DJ, Craig JR (1978) Mineral Chemistry of Metal Sulfides. Camb Univ Press

Vaughan DJ, Tossell JA (1980) The chemical bond and the properties of sulphide minerals: I. Zn, Fe and Cu in tetrahedral and triangular coordinations with sulfur. Can Mineral 18:157-163

Vaughan DJ, Tossell JA (1981) Electronic structure of thiospinel minerals: Results from MO calculations. Am Mineral 66:1250-1253

Vaughan DJ, Burns RG, Burns VM (1971) Geochemistry and bonding of thiospinel minerals. Geochim Cosmochim Acta 35:365-381

Vaughan DJ, Tossell JA, Johnson KH (1974) The bonding of ferrous iron to sulfur and oxygen: A comparative study using SCF-X_α scattered wave molecular orbital calculations. Geochim Cosmochim Acta 38:993-1005

von Oertzen GU, Jones RT, Gerson AR (2005) Electronic and optical properties of Fe, Zn and Pb sulfides. Phys Chem Mineral 32:255-268

Welz D, Rosenberg M (1987) Electronic band structure of tetrahedral iron sulfides. J Phys C 20:3911-3924

Wilson JA (1972) Systematics of the breakdown of Mott insulation in binary transition metal compounds. Adv Phys 21:143-198

Wincott PL, Vaughan DJ (2006) Spectroscopic studies of sulfides. Rev Mineral Geochem 61:181-229

Wintenberger M (1962) Etude électrique et magnétique de composés sulfurés et arséniés d'éléments de transition. III Propriétés électriques et magnétiques et liaisons dans l'arsenopyrite, la cobaltite et la loellingite. Bull Soc Fr Mineral 85:107-119

Womes M, Karnatak RC, Esteva JM, Lefebvre I, Allan G, Olivier-Fourcade J, Jumas JC (1997) Electronic structures of FeS and FeS_2: X-ray absorption spectroscopy and band structure calculations. J Phys Chem Solids 58: 345-352

Wright KV, Jackson RA (1995) Computer simulation of the structure and defect properties of zinc sulfide. J Mat Chem 5:2037-2040

Wright KV, Gale JD (2004) Interatomic potentials for the simulation of the zinc-blende and wurtzite forms of ZnS and CdS: bulk structure, properties, and phase stability. Phys Rev B 70:035211

Wright KV, Watson GW, Parker SC, Vaughan DJ (1998) Simulation of the structure and stability of sphalerite (ZnS) surfaces. Am Mineral 83:141-146

Zadjel P, Kisiel A, Zimnal-Starnawska M, Lee PM, Boscherini F, Giriat W (1999) XANES study of sulphur K edges of transition metal (V, Cr, Mn, Fe, Co, Ni) monosulphides: experiment and LMYO numerical calculations. J Alloys Comp 286:66-70

Zeng H, Schelly ZA, Ueno-Noto K, Marynick DS (2005) Density functional study of the structure of lead sulfide clusters $(PbS)_n$ (n = 1 - 9). J Phys Chem A 109:1616-1620.